Journal of Structural Geology 183 (2024) 105144

Contents lists available at ScienceDirect

Journal of Structural Geology

journal homepage: www.elsevier.com/locate/jsg

In-situ rock shattering and strain localization along a seismogenic fault in dolostones (Monte Marine fault, Italian Central Apennines)

S. Cortinovis [a], M. Fondriest [b], F. Balsamo [a,*], A. Lucca [a], F. La Valle [b], M. Pizzati [a], F. Storti [a], G. Di Toro [b,c]

[a] Dipartimento di Scienze Chimiche, della Vita e della Sostenibilità Ambientale, Università di Parma, 43124, Parma, Italy
[b] Dipartimento di Geoscienze, Università degli Studi di Padova, 35131, Padua, Italy
[c] Istituto Nazionale di Geofisica e Vulcanologia, 00143, Rome, Italy

ARTICLE INFO

Keywords:
In-situ shattered rocks
Off-fault deformation
Fault core
Seismogenic faults
Mosaic breccia
Carbonate faults

ABSTRACT

In-situ shattered rocks are often associated with seismogenic fault zones, but their mechanism of formation is still matter of debate, partly because of the limited number of field studies. Here we describe the characteristics of *in-situ* shattered rocks distribution along the NW-SE-striking seismogenic Monte Marine Fault (MMF) in the Italian Central Apennines. In the studied area, the MMF cuts through Mesozoic carbonates, is exhumed from <3 km depth and consists of two >5 km-long major hard-linked segments with normal kinematics. The linkage between the two fault segments occurs along a ~2 km-long step-over zone with E-W trending faults and oblique-slip kinematics. To the northwest, fault-related shear deformation is localized in a ~5 m-thick cataclastic fault core and off-fault deformation is dominated by *in-situ* shattered rocks up to ~40 m-thick. Instead, in the step-over zone to the southeast, the *in-situ* shattered rocks are up to ~500 m thick, particularly where MMF crosscuts older low-angle thrust faults.

We integrated detailed field structural surveys with microstructural and grain size distribution analyses of the fault rocks to assess the mechanism of (1) formation of *in-situ* shattered rocks and, (2) progressive localization of shear deformation along the MMF. The obtained results, after the viability of several formation mechanisms (mechanical models) have been reviewed, support the hypothesis that the formation of *in-situ* shattered rocks was associated with the propagation of (multiple) seismic ruptures (mainshocks and aftershock sequences) within a mechanically heterogeneous fault zone. Heterogeneity is due to the occurrence of preexisting damage related to previous earthquakes, but also inherited from the older low-angle thrust faults. Therefore, we suggest that the origin of these shattered rocks is more compatible with seismic related processes than only with quasi-static fault growth models. On the other hand, the cataclastic fault core derived from the progressive accommodation of shear deformation within the *in-situ* shattered rock volumes during several seismic cycles. We conclude that the large volumes of *in-situ* shattered rocks are the result of seismic-related dissipative processes in a geometrically and mechanically heterogeneous fault zone. In this scenario, large volumes of *in-situ* shattered rocks are compliant low velocity zones which can influence the propagation of earthquake ruptures.

1. Introduction

Fault zones are heterogeneous and structurally anisotropic mechanical discontinuities in the upper crust, able to control fluid flow and seismicity (e.g., Caine et al., 1996). They include a damage zone and one or more fault cores (Faulkner et al., 2010). In carbonates, fault damage zones are up to hundreds meters thick, accommodate limited slip displacement and are organized in fracture and subsidiary fault sets that may enhance fluid circulation (Micarelli et al., 2003; Storti et al., 2003; Kostakioti et al., 2004; Agosta and Aydin, 2006; Frost et al., 2009; Hausegger et al., 2010; Savage and Brodsky, 2011; Choi et al., 2016; Balsamo et al., 2019). Instead, fault cores accommodate most of the fault slip displacement, usually in <1 cm-thick slip zones, and are generally made of gouge and cataclastic rocks (Sibson, 1977) of variable thickness, extending up to few tens of meters (Micarelli et al., 2006; Solum and Huisman, 2017). Cataclastic rocks typically form by the combination of

* Corresponding author.
E-mail address: fabrizio.balsamo@unipr.it (F. Balsamo).

https://doi.org/10.1016/j.jsg.2024.105144
Received 10 August 2023; Received in revised form 3 February 2024; Accepted 26 April 2024
Available online 27 April 2024

intragranular extensional fracturing, chipping and shear fracturing (Billi and Storti, 2004; Storti et al., 2007; Cilona et al., 2019), plus pressure-solution and precipitation processes which contribute to enhance particle comminution and reduce rock porosity and permeability (Renard et al., 2000; Storti et al., 2003; Gratier et al., 2013; Clemenzi et al., 2015).

In the last decade, several authors described anomalous thickness of intensely fractured to fragmented rocks along fault damage zones in carbonate rocks (e.g., Fondriest et al., 2015, 2017; Schröckenfuchs et al., 2015; Demurtas et al., 2016; Ferraro et al., 2018; Fondriest et al., 2020). In these cases, fault-related deformation was classified as *in-situ shattering* and affected large rocks volumes by pervasive extensional fracturing down to the sub-millimetric scale (Agosta and Aydin 2006; Fondriest et al., 2015; Schröckenfuchs et al., 2015), thus resembling *pulverized rocks* produced by earthquake ruptures propagation in crystalline protoliths (granitoids and gneiss, e.g., Rockwell et al., 2009; Mitchell et al., 2011; Rempe et al., 2013). *In-situ* shattered and pulverized rocks are characterized by distinct textural patterns (e.g., particle size and shape distributions, microfracture density) compared to typical "frictional" fault rocks such as gouges and cataclasites, and are usually associated with large badland morphologies excavated in these incohesive densely fragmented materials (Mitchell et al., 2011; Fondriest et al., 2015; Schröckenfuchs et al., 2015; Aben et al., 2017). Despite reports of *in-situ* shattered fault rocks in several active tectonic settings, the mechanisms of their formation and the factors controlling their distribution along seismogenic faults in carbonate rocks are still poorly investigated.

In this study, we describe different types of fault rocks and document their thickness variations along the seismically active Monte Marine Fault (MMF) by combining detailed field mapping with structural, microstructural, particle size and shape data. The MMF is a seismogenic NW-SE trending extensional fault system cutting through Mesozoic carbonates exposed in the Monte Marine massif, on the eastern flank of the Upper Aterno River Valley, NW of L'Aquila town, in the Central Apennines (Fig. 1a). The last fault rupture occurred during the 1703 seismic sequence (mainshock of Mw 6.7; Moro et al., 2002, 2016; Galli et al., 2011; Falcucci et al., 2015). The MMF is characterized by an ultracataclastic to cataclastic fault core and large volumes of loose mosaic breccias (*sensu* Mort and Woodcock, 2008) preserved in the footwall block and interposed between the fault core and the fractured damage zone. These mosaic breccias resemble the *in-situ* shattered rocks described in other fault zones in carbonates (Mitchell et al., 2011; Fondriest et al., 2015; Schröckenfuchs et al., 2015; Aben et al., 2017; Billi et al., 2023).

The aims of this work are: (1) to classify and map the different fault rock types along the MMF; (2) to describe the overall structural architecture of the fault zone; (3) to discuss the origin of the loose mosaic breccias and the mechanism of progressive shear strain localization along the MMF; and (4) to investigate the role of inherited structures and preexisting damage in controlling the spatial distribution of off-fault deformation.

2. Geological setting

2.1. The Central Apennines and the Upper Aterno River Valley

The Central Apennines of Italy belong to the Late Oligocene to Present fold-and-thrust belt related to the W-subduction of the Adria plate beneath the European plate (Boccaletti et al., 1971; Doglioni, 1991; Carminati et al., 2004, Carminati and Doglioni, 2012). In the western sector of the Central Apennines, NE-verging thrusts are cut by NW-SE striking seismically active extensional fault zones. In this context, the Upper Aterno River Valley (Fig. 1) is a part of the Central Apennines Fault System (CAFS; Tondi and Cello, 2003), also known as Central Apennines Downfaulted Area (CADA; Ghisetti and Vezzani, 1999; Agosta and Aydin, 2006). This region was affected by the continuous

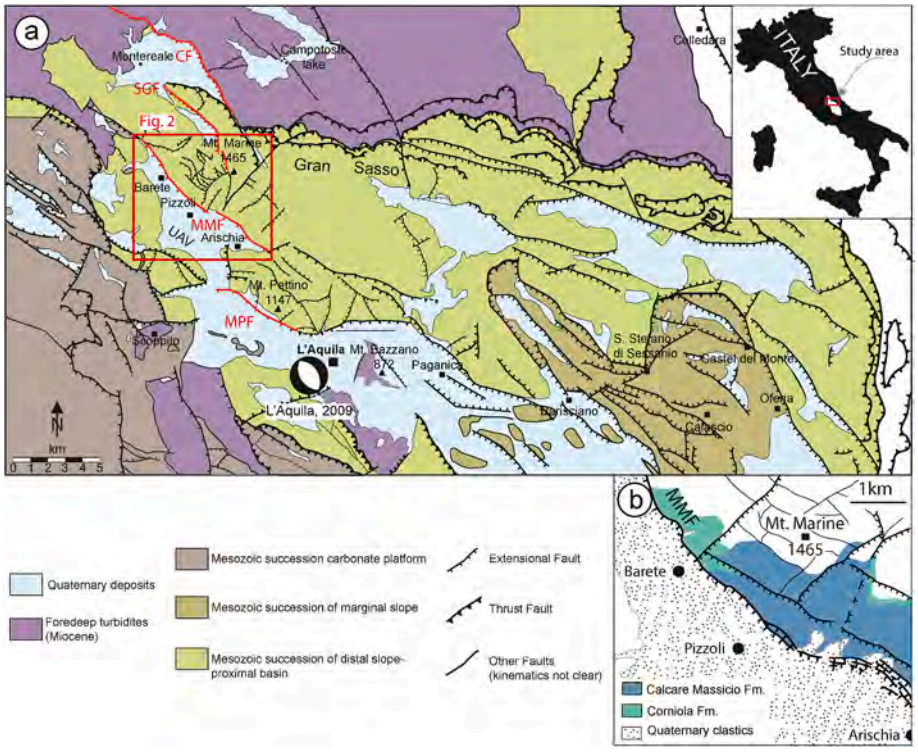

Fig. 1. Geological setting of the studied seismogenic fault. (a) Simplified geological map of the Central Apennines: MMF indicates the Mt. Marine Fault, MPF the Mt. Pettino Fault, SGF the San Giovanni Fault, and CF the Capitignano Fault; inset in the upper right corner show location of the study area within the Central Apennines Downfaulted Area (from Ghisetti and Vezzani, 1999). (b) Simplified sketch of the MMF showing the main fault surface, secondary normal faults, thrusts, and exposed Formations in the footwall block (from Servizio Geologico d'Italia, F. 348, 2022).

deepening of the hydrographic network (Galli et al., 2011), and related continental basin excavation, and was later dissected by extensional faulting during the Quaternary (Agosta and Aydin, 2006; Ferrarini et al., 2015; Lavecchia et al., 2022). The actual configuration of the Upper Aterno River Valley consists of a NW-SE trending Quaternary basin bordered by NW-SE striking seismogenic extensional fault zones characterized by *en-échelon* over-stepping geometries. They correspond, from the south to the north, to the Mt. Pettino Fault, the Mt. Marine Fault, the S. Giovanni Fault and the Capitignano Fault (Fig. 1a). These fault segments shaped the northeastern flank of the Upper Aterno River Valley (Galadini and Messina, 2004) and have been entirely or partially activated during the 1703 (mainshock Mw 6.7) and the 2009 L'Aquila (mainshock Mw 6.1) seismic sequences (Chiaraluce et al., 2011; Galli et al., 2011; Lavecchia et al., 2012; Moro et al., 2016; Pizzi et al., 2017; Falcucci et al., 2018; Pucci et al., 2019).

2.2. The Monte Marine Fault

The MMF (Fig. 1a) is located in the NE border of the Upper Aterno River Valley, and affect partially dolomitized Mesozoic carbonate rocks of the Adria passive margin succession, extensively exposed in its footwall block. In particular, the fault zone cuts through the poorly layered

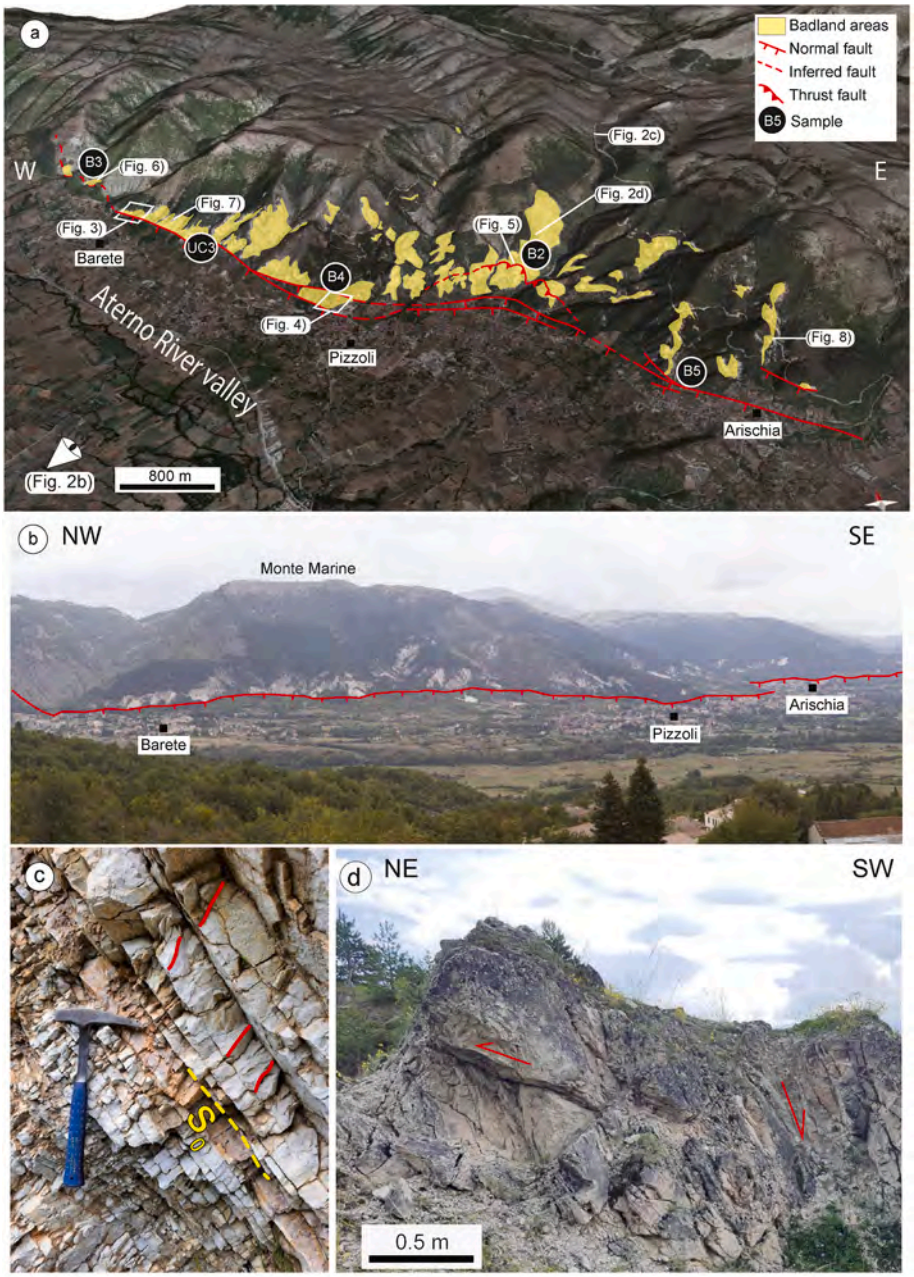

Fig. 2. Overview of the Monte Marine Fault and studied localities. (a) Perspective aerial view (Google Earth) illustrating the along-strike architecture of the MMF and the extent of the badland morphologies (in yellow) in the footwall damage zone. (b) Panoramic view of the NW segment of the MMF seen from the SW; location of photograph is shown in (a). (c) Example of the steeply dipping, well-bedded Corniola Formation host rock far from the Monte Marine Fault, affected by bed-perpendicular pressure-solution cleavage associated with the compressional phase; bedding in yellow (S_0) and cleavage in red. Hammer for scale is 31.8 cm. (d) Example of the massive dolomitized Calcare Massiccio Formation affected by reverse faults with S–C fabric indicating top-to-the-NE kinematics. Steeply dipping normal faults generally overprint thrust faults. (For interpretation of the references to color in this figure legend, the reader is referred to the Web version of this article.)

platform limestone of the Calcare Massiccio Formation (Early Jurassic) to the South and the overlying, well-bedded basinal limestone pertaining to the Corniola Formation (Early Jurassic) near Barete village to the North, and passing upwards to Late Jurassic and Cretaceous rocks moving towards the NW fault tip (Fig. 1b). Recent geological cartography documented the presence of a Jurassic extensional tectonic phase in the Monte Marine area, as highlighted by the presence of reduced succession (Bugarone Fm.) overlying the Calcare Massiccio Formation (Servizio Geologico d'Italia, sheets 348–349 available at https://www.isprambiente.gov.it/Media/carg/abruzzo.html). Another feature associated with Jurassic tectonics is the dolomitization of the Jurassic Formations imparted by fluid circulation across synsedimentary fault zones.

The present-day MMF originated in Late Pliocene times, when contractional deformations in this region of the Central Apennines were overprinted by extensional tectonics (Cosentino et al., 2017; Servizio Geologico d'Italia, 2010; Servizio Geologico d'Italia, 2022). The MMF, overall, is ~14 km long (Galli et al., 2011) and was activated during the February 2nd, 1703 Mw 6.7 earthquake, which caused hundreds of casualties in the Aterno Valley and in the town of L'Aquila. Based on paleoseismological studies, the seismically active segment of the Monte Marine fault is ~8 km long and extends from the Barete village to the Arischia village (Blumetti, 1995; Moro et al., 2002; Galli et al., 2011). Along this segment, the footwall block of the fault zone is lined by continuous badland morphologies developed into poorly cohesive fragmented carbonates, and extending at distances >1 km from the principal fault trace NE of the Arischia village, (Fig. 2a and b). The complex paleoseimological history of the MMF is well documented (Moro et al., 2002, 2016; Galli et al., 2011; Falcucci et al., 2015), with at least five surface rupture events after the 6th-5th millennium B.C. (maximum recurrence interval of 7000 years; Calamita and Pizzi, 1992; Cello et al., 1997; Galadini and Galli, 2000; Galli et al., 2011; Falcucci et al., 2015; Moro et al., 2016).

3. Methods

3.1. Field mapping and structural analysis

We mapped a representative area of interest (near the village of Barete) located in the footwall of the main fault surface (Fig. 2a) at 1:500 scale. Field mapping, based on orthorectified aerial photographs available on the website of the Regione Abruzzo (http://geoportale.regione.abruzzo.it/Cartanet), was aimed at (1) mapping the fault zone structural units (fault core rocks and fractured rock masses, according to the classification of Sibson, 1977, and Mort and Woodcock, 2008), (2) the

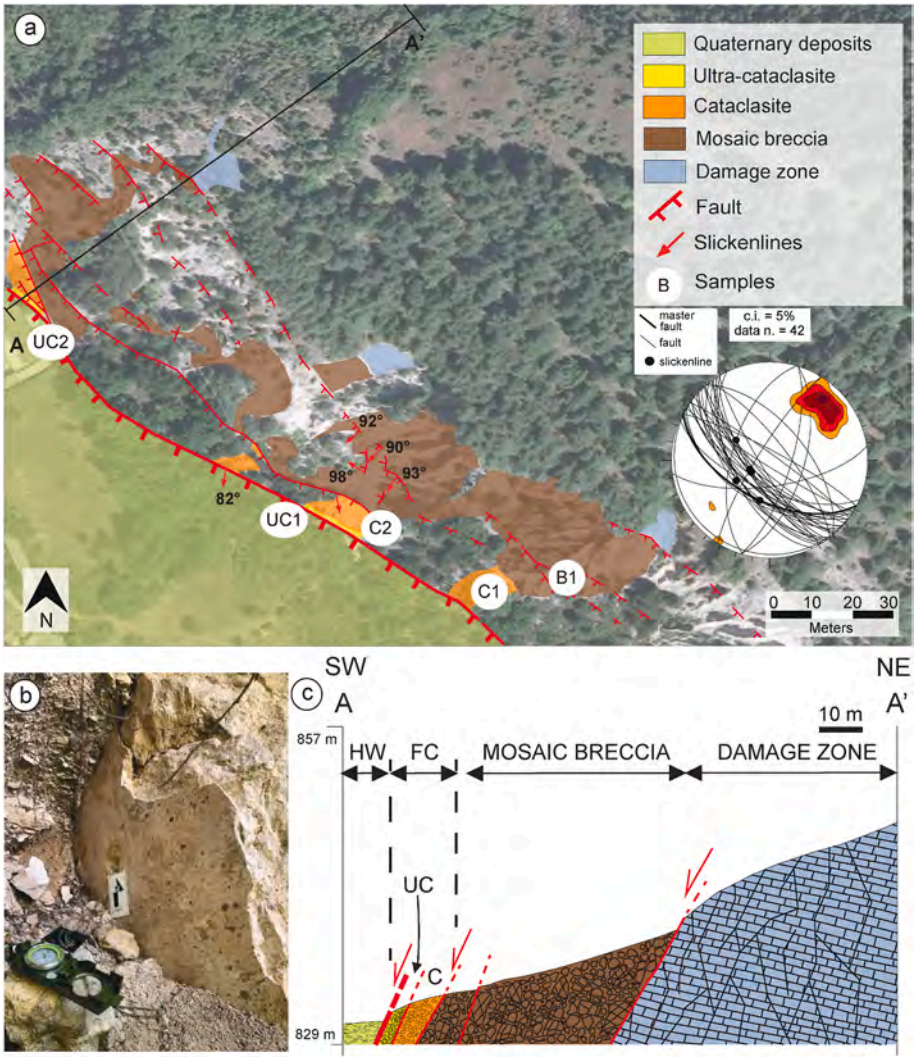

Fig. 3. Geological map and cross-section of the fault rock types along the MMF, near the village of Barete. (a) Map showing the distribution of fault core rocks and mosaic breccias, with position of samples. Structural data measured in this area are shown in the stereonet (Wulff-lower hemisphere). (b) Example of polished main fault surface juxtaposing Quaternary deposits in the hanging wall with dolostone ultracataclasites in the footwall. (c) Cross section showing the main structure of the MMF in this sector. Vertical exaggeration of 2*X*. HW, hanging wall; FC, fault core; UC, ultracataclasite; C, cataclasite.

principal and subsidiary faults, (3) measuring fault attitudes and kinematic indicators, and (4) to collect fault rock samples for petrographic-microstructural observations and quantitative image analyses. Based on the detailed map, we constructed a ~80 m-long geological cross-section through the fault zone (Fig. 3). A total of 862 structural data were collected. Fault kinematics was measured on slickensides preserved both on the principal and subsidiary fault surfaces. Field observations, combined with microstructural and image analyses, provided the basis to classify fault rocks in the different structural domains (see section 4).

3.2. Microstructural analyses

Fifty-eight thin sections were analyzed under a petrographic microscope. Samples were first impregnated with epoxy resin and then sectioned perpendicular to the fault surfaces and parallel to slickenlines to obtain oriented standard (~30 μm-thick) petrographic polished thin sections. Petrographic observations were performed with a Zeiss Axioplan 2 optical microscope. Selected samples were observed with a JEOL JSM 6400 Scanning Electron Microscope (SEM), at different magnifications, to examine microstructures within the mm-thick localized slip zones. Energy dispersion spectroscopy (EDS) analyses were performed to distinguish dolomite from calcite and to identify minor chemical elements.

3.3. 2D particle size and shape analyses

Cohesive fault rock samples were impregnated with epoxy resin for thin section preparation. Five thin sections were analyzed by means of image analysis to calculate particle size and shape distributions of ultracataclastic and cataclastic fault core domains, and one sample slab was selected as representative for the *in-situ* shattered mosaic breccias. We acquired thin section scans with a Nikon Supercool Scan 5000. We analyzed the entire thin section areas (36.5 × 24 mm) at 13,134 × 9449 pixels resolution to get comparable datasets for all the samples. Given the large dimensions of the cohesive mosaic breccia (30 × 20 × 15 cm), this rock sample was cut with a diamond wire to obtain a fresh surface available for image analysis. In this case, we manually traced all the recognizable clast boundaries on the polished fresh cut (each clast is delimited by opening-mode fractures) on a transparent paper that was scanned to obtain a digitized image of the breccia texture. Particle perimeters were manually digitized using ImageJ (version 1.53 S) image analysis software to calculate their areas (Schneider et al., 2012). Grain size and shape data were obtained from particle areal data (Heilbronner and Keulen, 2006). Actually, we calculated the equivalent diameter value D_{eq}, corresponding to the diameter of a circular particle with the same area A of the analyzed particle, using:

$$D_{eq} = 2 * \sqrt{\frac{A}{\pi}} \quad (1)$$

For each sample, we sorted particles in size classes according to the Udden-Wentworth scale (Wentworth, 1922) to build a graph where the number of particles is plotted versus the logarithm of particle size. We also plotted in a Log-Log diagram the cumulative number of particles versus the particle size, thus obtaining the fractal dimension (D-value), which is calculated as the slope of the best-fit power-law distribution between particle size and cumulative frequency of particles for each particle size class (Turcotte, 1986; Blenkinsop, 1991; Rawling and Goodwin, 2003; Balsamo and Storti, 2011). The fractal dimension was used to quantify the comminution intensity of variably fragmented rocks (Storti et al., 2003).

For particle shape analysis, we used Aspect Ratio (AR) and Circularity (C) values. Aspect Ratio describes the elongation of particles and is defined by:

$$AR = \frac{\text{Lenght max axis}}{\text{Lenght min axis}}, \quad (2)$$

where max *axis* and min *axis* indicate the longest and shortest axes of the ellipse that best approximates the area of the clast, respectively. Aspect Ratio may range from 1 (perfect isotropic particle) up to infinity (elongate and anisotropic particle). Circularity indicates the roughness of the perimeter of particles and can be calculated as follows:

$$C = \frac{4\pi\ \text{A}}{\text{Perimeter}^2}, \quad (3)$$

where A stands for the surface of the digitized clast and *Perimeter* represents the length of the clast outer boundary. Circularity values span from 1 (perfect circular shape) to 0 (particle strongly deviating from perfect circle). Values of Aspect Ratio and Circularity were calculated from the software ImageJ. The normalized frequency of particle Aspect Ratio and Circularity, in the range between 62.5 μm and 16 mm, are plotted in frequency distribution histograms. Mean values of Aspect Ratio and Circularity are calculated by best fitting Gaussian normal distributions to frequency distributions.

3.4. 3D particle size distribution analysis

Poorly cohesive to incohesive fault rock samples were analyzed through 3D laser diffraction granulometry, following the workflow proposed by Storti and Balsamo (2010). An ultracataclasite sample and three samples of *in-situ* mosaic breccia were first dried at a constant temperature of 45 °C for 48 h, and then passed through a 2000 μm sieve to remove larger particle. Particle size analysis was performed with a Mastersizer 3000 (Malvern Panalytical) laser diffraction granulometer having an operating size range spanning from 0.01 to 3500 μm. In particular, we used the Aero S air dispersion unit, which uses a vibrating sample holder and negative air pressure to disperse the material. Different air pressures and vibration intensities were tested on the four representative samples in order to obtain excellent reproducibility. Based on the particle size distribution curves, as for 2-Dimensional particle size analysis, mean particle size, mode, and fractal dimension (D-value) were calculated. Therefore, we used D to quantify relative textural differences between fault rocks and to discuss possible deformation mechanisms accounting for such distributions (Mandelbrot, 1977; Turcotte, 1986; Sammis et al., 1987).

4. Results

4.1. Overall fault architecture

The structural architecture of the MMF varies significantly along strike. Overall, the fault zone is NW-SE oriented and consists of two main fault segments that are hard-linked by E-W subsidiary fault segments in the central part of the fault zone, near the village of Pizzoli (Fig. 2a). The NW fault segment has a planar geometry and is lined by a badland area with a nearly constant width of ~30–40 m northeast of the Barete village. The width of the badland morphologies, excavated in poorly cohesive fault rocks, increases southeastward, up to >500 m from the principal fault surface, approaching the step-over zone northeast of the Pizzoli village. A further increase in the width of badland morphologies is observed near the SE fault segments and reaches a maximum of ~1 km away from the principal fault trace northeast of the village of Arischia (Fig. 2a). In this study, we first focus on the NW fault segment and describe in detail a cross-section of the MMF northeast of the Barete village. Then, additional field observations and structural measurements were collected moving toward SE in the step-over zone (Fig. 2a and b). Out of the badland morphologies associated with the MMF, the host rock consists of (i) folded Corniola Formation limestone, affected by bed-orthogonal pressure-solution cleavage (Fig. 2c), and (ii) faulted and

fractured Calcare Massiccio Formation limestone associated with secondary NE-verging thrusts (Fig. 2d).

Along the NW segment, the fault zone cuts through the Calcare Massiccio and the Corniola Formation (Vezzani and Ghisetti, 1998; Servizio Geologico d'Italia, 2010; Servizio Geologico d'Italia, 2022; inset in Fig. 1b). The mean attitude of the principal fault surface, which crops out discontinuously along the fault zone, is 204°/65° (dip direction/dip; Fig. 3a and b). Slickenlines indicate dip-slip extensional kinematics (Fig. 3a). In the footwall block, the principal fault surface borders a 5–10 m-thick fault core made of a ~2 m-thick layer of whitish and cohesive ultracataclasites (Fig. 3b and c), gradually passing to a 2–8 m-thick domain of yellowish, foliated cataclasites (Fig. 3c). A 20–40 m-thick body of loose mosaic breccias is interposed between the damage zone and the cataclastic fault core. These breccias display heterogeneous clast sizes, host subsidiary faults, and locally contain meters-wide cohesive lenses of intensely fractured rocks preserving the primary sedimentary features (e.g., bedding) embedded in an incoherent, loose fractured material. The transition from the mosaic breccias to the damage zone is either transitional or, more frequently, marked by sharp contacts along synthetic extensional faults with dip-slip kinematics (Fig. 3c).

Towards the southeast, near the Pizzoli village, the fault zone is structurally more complex. Here, the principal fault surface strikes ~ E-W and cuts through the dolomitized Calcare Massiccio Formation. In particular, in the step-over zone we documented a significant increase in the thickness of the mosaic breccia volume. This large volume originated the badland morphologies described above (see Fig. 2a), which extend up to 500–600 m away from the principal fault surface. In this area, we recognized the same fault rock types moving away from the principal fault surface, i.e., ultracataclasites, foliated cataclasites with subsidiary extensional faults (Fig. 4a), mosaic breccias (Fig. 4b and c), and the fractured damage zone (Fig. 4d). Here, subsidiary extensional faults are more scattered compared to the Barete site, and are mostly organized in NW-SE to E-W sets (Fig. 4e). Fault slickenlines indicate dip-slip and also oblique kinematics with pitch values comprised between 50° and 130° (Fig. 4f). Low-angle thrust faults are also present and are organized in conjugate sets with mean attitude of 206°/26° and 042°/24°, respectively (Fig. 4g). Slickenlines on thrust faults indicate multiple transport directions: NNE-SSW, oblique, and along-strike on lateral ramps (Fig. 4h). Low-angle reverse faults are dislocated by NW-SE extensional faults (Fig. 5). We documented local increases in the volume and intensity of fault rock deformation (from mosaic breccias to ultracataclasites) at the intersection between extensional faults and older thrust faults (Fig. 2a and 5). The damage zone consists of fractured rocks and subsidiary synthetic and antithetic, NW-SE to E-W striking, extensional faults, as well as minor NE-SW striking ones.

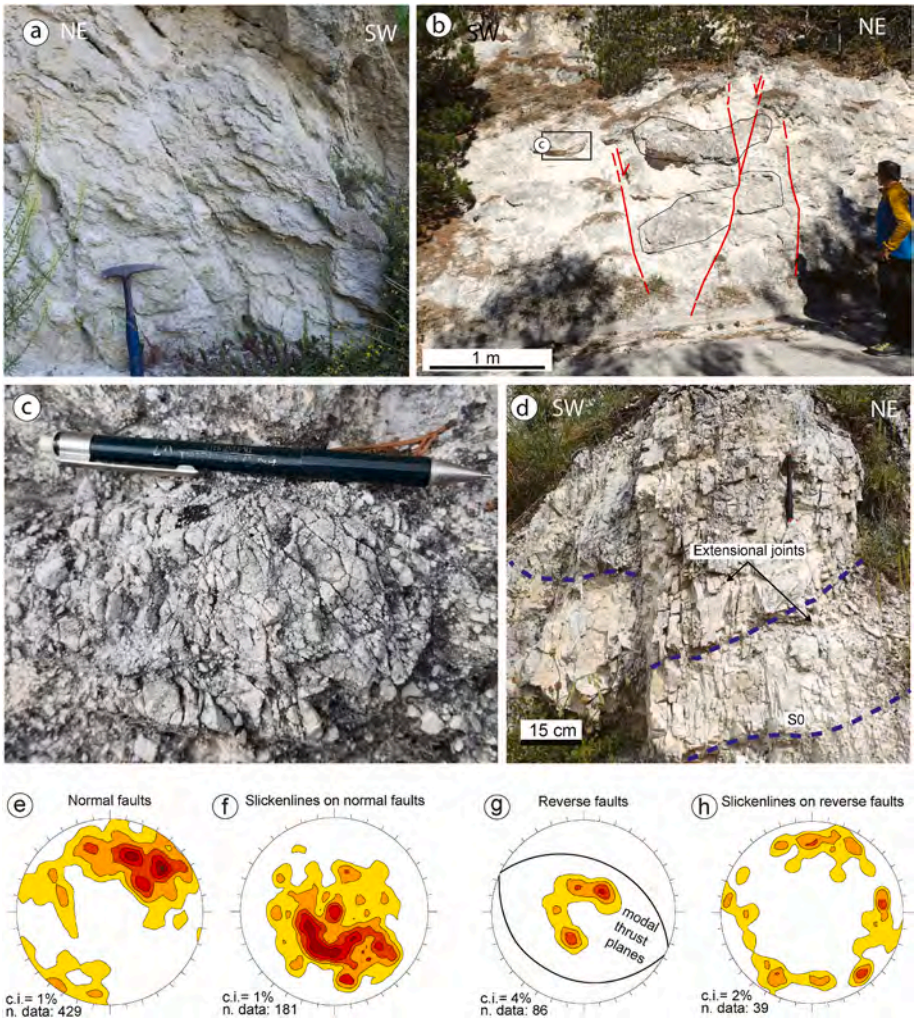

Fig. 4. Fault core, mosaic breccia and damage zone characteristics in the Calcare Massiccio Formation near the village of Pizzoli. (a) Foliated cataclasite forming extensional S–C fabric in the fault core. (b) Breccias with remnants of coherent lithons in the footwall of the MMF. (c) Detail of partially cohesive brecciated rocks. (d) Closely-spaced, subparallel joints developed in the footwall damage zone. (e–h) Stereonets (Wulff-lower hemisphere) showing structural data on normal (e, f) and reverse (g, h) faults measured in the area of the Pizzoli village.

Fig. 5. Field image showing the cross-cutting relationships between thrust faults and minor extensional faults in the over-step area (Sant'Antonio canyon, Marruci locality). Thrust faults orientation and kinematics are shown in the stereographic projection (lower hemisphere). In this site, located about 500 m far from the main fault surface, the Calcare Massiccio Formation is still pervasively brecciated.

4.2. Mesoscale description of fault rocks

In a typical cross-sectional architecture of the MMF, the principal fault surface (master fault in Fig. 6a) has a positive relief with respect to the underlying cataclastic rocks and is locally covered by deformed and partially cemented Quaternary slope deposits (Fig. 6b). Contrasts in textures, colours, and relief at the outcrop scale, allowed us to group fault rocks in ultracataclasites and cataclasites (fault core units, Fig. 6c and d), mosaic breccias (Fig. 6e), and variably fractured damage zone units (high- and low-strain damage zone).

4.2.1. Ultracataclasites

Ultracataclasites consist of white fine-grained and cohesive fault rocks, matrix-supported, with few sub-rounded survivor grains (up to 4–5 mm in diameter), made mostly of dolomite and minor calcitic bioclasts, vein fragments, and rare chert, floating in a light grey to brownish matrix (Fig. 6c). The content of bioclasts and chert with respect to dolomite clasts is significantly higher in the northwest fault segment, where the MMF cuts through the Corniola Formation, rather than in the Pizzoli area (step-over zone) to the southeast, where the fault affects the extensively dolomitized Calcare Massiccio Formation. Ultracataclasites are mostly localized along the principal slip zone of the MMF (1–2 m-

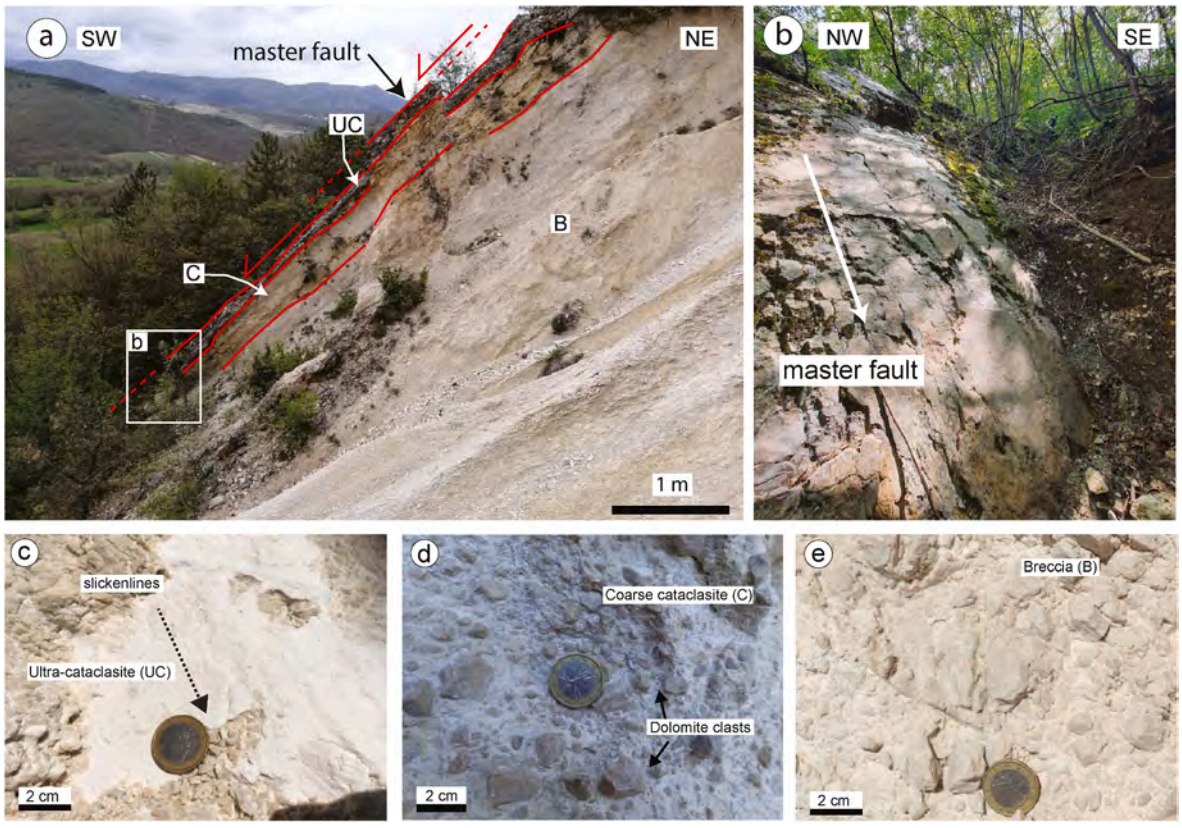

Fig. 6. Fault zone structure and related fault rocks. (a) Outcrop photographs of the Monte Marine Fault near Barete village showing different adjacent structural domains (fault core and breccias). (b) The master fault plane in contact with Quaternary deposits is highly weathered; white arrow indicates the direction of striae on the master fault plane. (c) Close view of fine-grained ultracataclasites, (d) coarse-grained cataclasites and (e) mosaic breccias. UC, ultracatclasite; C, cataclasite; B, mosaic breccia.

thick layer) and are, in places, cut by small faults with well-developed kinematic indicators. Subsidiary ultracataclastic slip zones are also found in the nearby cataclastic domain and lining some of the subsidiary fault strands developed within the breccia and damage zone units.

4.2.2. Cataclasites

Cataclasites consist of light grey to yellowish, fine-grained and partially incohesive fault core rocks composed of very fine-grained matrix with sub-rounded and brownish dolomite survivor grains 1–10 mm in size, composing up to half the rock bulk volume (Fig. 6d). Overall, cataclasites are foliated and form up to ~2–8 m-thick layers along the master fault in the Barete area (Fig. 7a). This cataclastic domain includes also subsidiary slip surfaces. The transition between foliated cataclasites and breccias is generally very sharp along subsidiary extensional faults (Fig. 7b), although patches of protocataclasites are locally observed at the transition between the fault core and the loose mosaic breccias.

4.2.3. Mosaic breccias

Mosaic breccias (*sensu* Mort and Woodcock, 2008) are formed by very angular, micrometric to sub-centimetric dolomite grains characterized by a jigsaw texture and affected by a network of randomly oriented tensile fractures. Mosaic breccias developed in the well-layered Corniola Formation along the northwest fault segment (Fig. 7) are locally sealed by a network of whitish calcite veins, in contrast with breccias occurring in the Calcare Massiccio Formation to the southeast, which are typically highly incohesive to loose (Fig. 8a and b). Mosaic breccias show different textural characteristics compared to the fault core rocks. The main textural differences include the occurrence of pervasive extensional fracturing down to the microscale with radial to highly scattered fracture patterns, and the characteristic jigsaw-fit texture defined by rock fragments with no evidence of translation and rotation from the meso-to the microscale (Fig. 8c). These textural characteristics suggest the absence of significant shear deformation. This is further supported by the preservation of primary sedimentary fabrics, such as bedding, stromatolitic layering in the Calcare Massiccio Formation and the flattened chert nodules in the Corniola Formation (Fig. 7a and c). Northeast of the Barete village, along the NW fault segment, the 10–40 cm-thick beds of the Corniola Formation are still well visible into the mosaic breccias; they are gently folded and progressively dragged toward the principal fault surface (Fig. 7a), reaching a dip of 40–50° in the proximity of the cataclastic fault core. Such brecciated and dragged beds are dissected by subsidiary extensional faults at the contact with the fault core (Fig. 7b). Within the breccia, chert nodules parallel to bedding are flattened, stretched in the bedding-dip direction, pervasively fragmented and locally offset by minor conjugate extensional faults (Fig. 7c). When offset by minor faults, the fragmented chert nodules are smeared along the fault surface (Fig. 7e).

4.2.4. Damage zone

The damage zone of the MMF is characterized by fractured rock masses well preserving the original bedding (striking NW-SE and dipping 10–20° toward SW), cut by joints, small shear fractures, and subsidiary faults (Fig. 7d). The exposed damage zone is affected by fractures with spacing down to few centimeters at the transition with mosaic breccias, and fracture spacing increase up to 20–30 cm moving to the more external part of the MMF into the footwall (Fig. 7d). The fracture network affecting this damage zone is very distinct compared to that affecting the mosaic breccias. In fact, subvertical fractures in the damage zone have a preferential orientation parallel to the main fault and spacing between few cm to dm, while fractures in the breccia are randomly oriented and fracture density is so high that the material resemble a fine-to coarse-grained granular material (although some m-size lithons with fault-parallel fractures and surrounded by loose breccias are still visible, Fig. 8b).

4.3. Microstructural characterization of fault rocks

4.3.1. Fault core rocks and mosaic breccias

At the optical microscope, ultracataclasites are dominated by a matrix (≥90% of the volume) of very comminuted dolomite fragments and calcitic micrites and sparites. They contain heterometric, well-rounded clasts of dolomite, minor chert clasts, and bioclasts, up to 1–2 mm in size (Fig. 9a and b). In all the samples, we recognized a significant grain size reduction towards the slip surfaces.

Cataclasites are characterized by coarser survivor clasts of dolostone (2–3 mm in size, up to 10 mm), which are more angular than those in the ultracataclasites (Fig. 9c and d) and float in a fine-grained matrix mainly composed of fragments of dolostone and limestone. We also documented the presence of tectonic stylolites (Fig. 9c and d), defined by black Fe-oxides and other residual insoluble minerals (Fig. 9c).

In the mosaic breccia, the shape of the dolostone clasts significantly changes, and the amount of cataclastic matrix abruptly decreases with respect to ultracataclasites and cataclasites. Dolostone clasts have dimensions ranging from few hundreds of micrometers to few centimeters at maximum and display pervasive extensional fracturing without any evidence for rotation, translation or abrasion (Fig. 9e and f). Locally, mosaic breccias are sealed by randomly oriented white calcite veins (from sub-millimetric to ~4–5 mm-thick) (Fig. 9g).

4.3.2. Localized slip zones

Within cataclastic and ultracataclastic fault core domains, we recognized extremely localized slip zones associated with sharp, smooth to mirror-like surfaces (Fig. 10a) that are often truncating dolomitic ultracataclasites cemented by calcite (Fig. 10b). Calcite clasts, likely representing fragments of previous veins and cements, record cyclic fragmentation and sealing processes (Fig. 10c). Ultracataclasites are often characterized by grain size reduction toward slip surfaces and display both isotropic and mixed calcite-dolomite foliated fabrics (Fig. 10d). Some slip zones are characterized by flame-like structures consisting of highly comminuted material with convolute shapes (Fig. 10e). On top of some slip surfaces, layers of extremely comminuted dolomite-calcite clasts (size down to ~100 nm) were observed, as well as calcite veins growing with the crystals' major axis perpendicular to the slip surface (Fig. 10f).

4.4. Particle size distribution and fractal dimension

Particle size distributions in two-dimension were obtained by image analysis on cohesive samples using five scanned thin sections (representative of two ultracataclasites, two cataclasites, and one mosaic breccia as shown in Supplementary Materials S1) and one polished slab (representative of a mosaic breccia, Fig. 9g). Results from ultracataclasites and cataclasites (fault core domain) are shown in the left and central columns of Fig. 11, respectively, while results from mosaic breccias are plotted in the right column. Particle size data are plotted both as frequency distributions vs. log size classes (Fig. 11a–c) and cumulative frequency distributions vs. size class in bi-logarithmic graphs (Fig. 11d–e). Particle size distributions overall show unimodal curves. Ultracataclasites UC1 and UC2 have mean values of 272 and 139 μm, modal values of 124 and 80 μm, and median values of 185 and 113 μm, respectively (Fig. 11a). Cataclasites C1 and C2 are very similar to ultracataclasites, with mean values of 358 and 304 μm, modal values of 156 and 107 μm, and median values of 245 and 202 μm, respectively (Fig. 11b). Mosaic breccias have different frequency distributions with respect to the other two fault core rocks. For breccias B1 and B2, we calculated mean values of 819 and 3036 μm, modal values 182 and 889 μm, and median values 463 and 2714 μm, respectively (Fig. 11c). We recognize some differences even in the shape of the cumulative bi-logarithmic graphs. The curves of ultracataclasites and cataclasites are well fitted by power law linear best-fits between one and two orders of magnitude (Fig. 11d–e). Because of the minor number of clasts in the

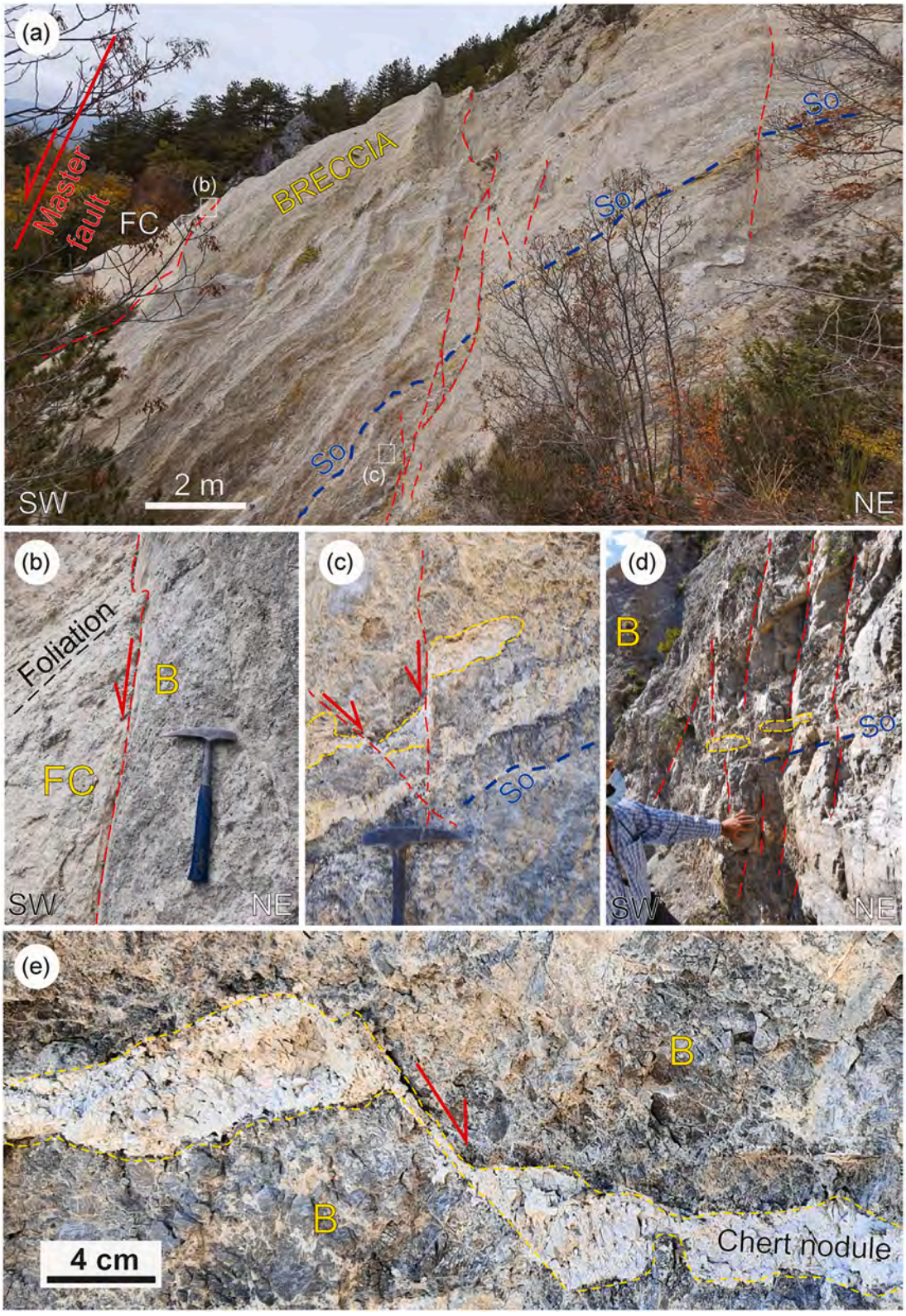

Fig. 7. Outcrop-scale features of mosaic breccias developed in the footwall block in well-layered dolomitized Corniola Formation, exposed near the village of Barete. (a) Example of the breccia domain, in a section orthogonal to the MMF, in which the bedding is clearly preserved (S_0), dragged towards the master fault surface and crosscut by secondary normal faults. (b) Sharp transition (minor normal fault) between foliated cataclasite in the fault core and breccias. (c) Flattened and stretched chert nodules (yellow dotted line) in the brecciated rocks oriented parallel to bedding, dislocated by secondary conjugate normal faults. (d) Densely fractured inner part of the damage zone at the transition with the mosaic breccias. (e) Detail of stretched and brecciated chert nodule, offset by a minor normal fault with a smear along the fault surface. FC, fault core; B, mosaic breccia; S_0, bedding.

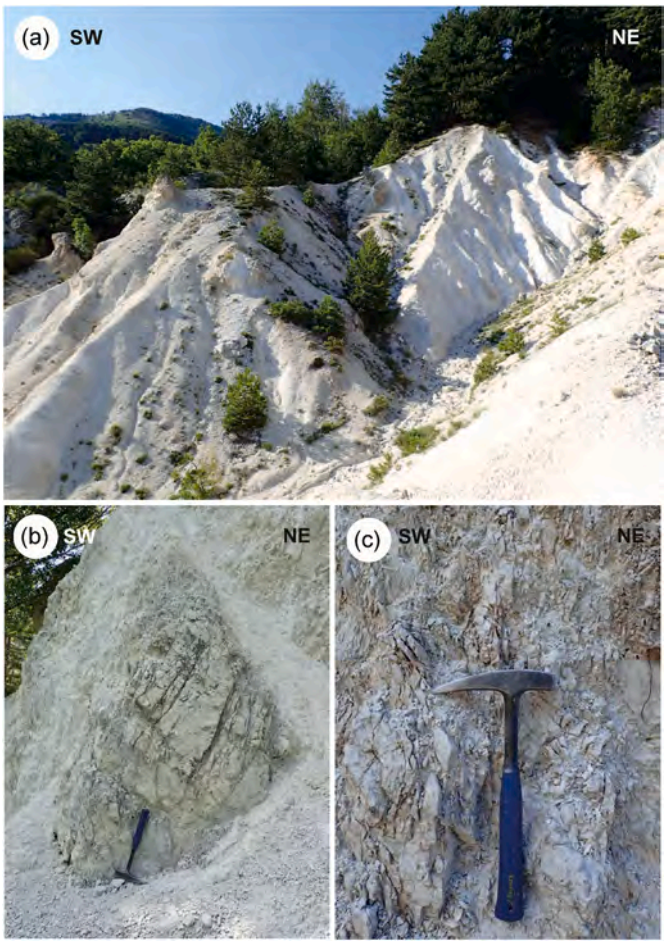

Fig. 8. Mesoscale features of mosaic breccias in the Calcare Massiccio Formation near the village of Arischia. (a) Badland morphology in a tens of m-wide outcrop of breccias. (b) Example of a still cohesive fractured lithon surrounded by intensity fragmented and loose breccias. Fractures within the lithon are subparallel to the main normal fault. (c) Example of jigsaw fit texture in the loose mosaic breccia with heterogeneous clast size distribution ranging from < 1 mm up to 5 cm.

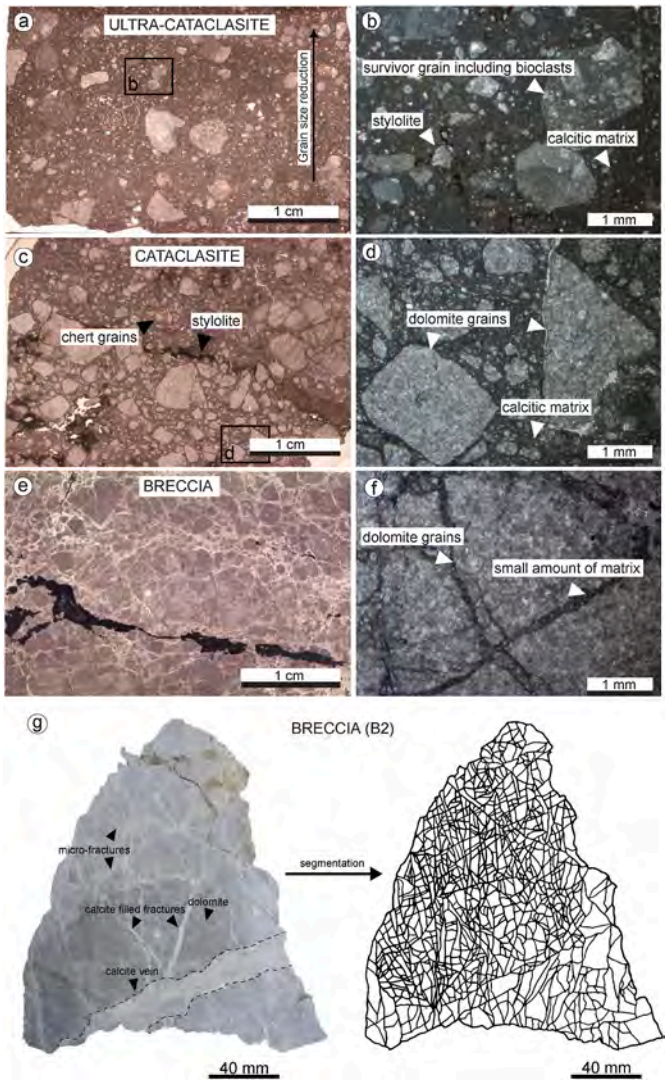

Fig. 9. Microtextural features of studied MMF rocks. (a) Thin section scans (TSS) and (b) plane polarized image (PPL) of ultracataclasites. (c–d) TSS and PPL of cataclasites. (e-f) TSS and PPL of a breccia sample. (g) Picture and line-drawing of fractures of a cohesive breccia sample collected in the outer part of the breccia domain.

coarse samples, the cumulative granulometric curves obtained from mosaic breccias present less particle size classes than the other domains and are less confidently interpolated (Fig. 11f). These differences in particle size distributions result in two-dimensional fractal value of $D = 1.05$ and 1.31 in mosaic breccias, $D = 1.63$ and 1.76 in cataclasites, and $D = 1.81$ and 2.13 in ultracataclasites. In all the analyzed thin sections we got a good correlation coefficient ($R^2 > 0.91$), while in the mosaic breccia slab sample the correlation coefficient is $R^2 = 0.78$.

Three-dimensional particle size distributions of poorly cohesive fault core rocks and mosaic breccias were determined via laser-granulometry technique on one ultracataclasite and three loose mosaic breccias. The particle size distributions of an ultracataclasite and of three mosaic breccias are plotted as frequency distributions on the left side of Fig. 12 (in volume density versus the logarithm of particle size graphs) and as log cumulative particle number versus logarithm of particle size graphs on the right side. The ultracataclasite sample UC3 shows a polymodal distribution characterized by a low sorting. Its mean value is 373 μm, the mode is 84 μm and the median is 82 μm (Fig. 12a). These values are comparable with ultracataclasites analyzed through image analysis in two-dimensions. The three loose mosaic breccia samples are characterized by consistently comparable unimodal frequency distributions with better sorting than the ultracataclasite sample, showing less than 2% of volume density for size classes <100 μm (Fig. 12b–d). Mean equivalent diameter values are 1130, 903 and 1020 μm, respectively for B3, B4 and B5. Their modal values are very consistent, at 1430, 1440 and 1420 μm and their median values are 1030, 694 and 881 μm, very close to the median values due to the high sorting and low skewness of the particle size distributions (Fig. 12b, c, d). Cumulative granulometric distributions of three-dimensional laser analyses are all well fitted by power laws with coefficient of linear regression with values $R^2 > 0.99$ across three orders of magnitude. The three-dimensional fractal dimensions are $D = 2.97$ for the ultracataclasite UC3 and $D = 2.52$, 2.50 and 2.51 for B3, B4 and B5, respectively (Fig. 12e–h).

4.5. Particle shape distributions

Particle shape distributions in Fig. 13 pertain to the same cohesive samples reported in Fig. 11 and Supplementary Material S1, divided by fault rock type (i.e., two ultracataclasites, two cataclasites and two mosaic breccias). We plotted the normalized particle number versus Aspect Ratio (Fig. 13a–c) and Circularity values (Fig. 13d–f), respectively. Ultracataclasites and cataclasites are characterized by a narrow frequency distribution of aspect ratios, with a maximum value $AR < 4$.

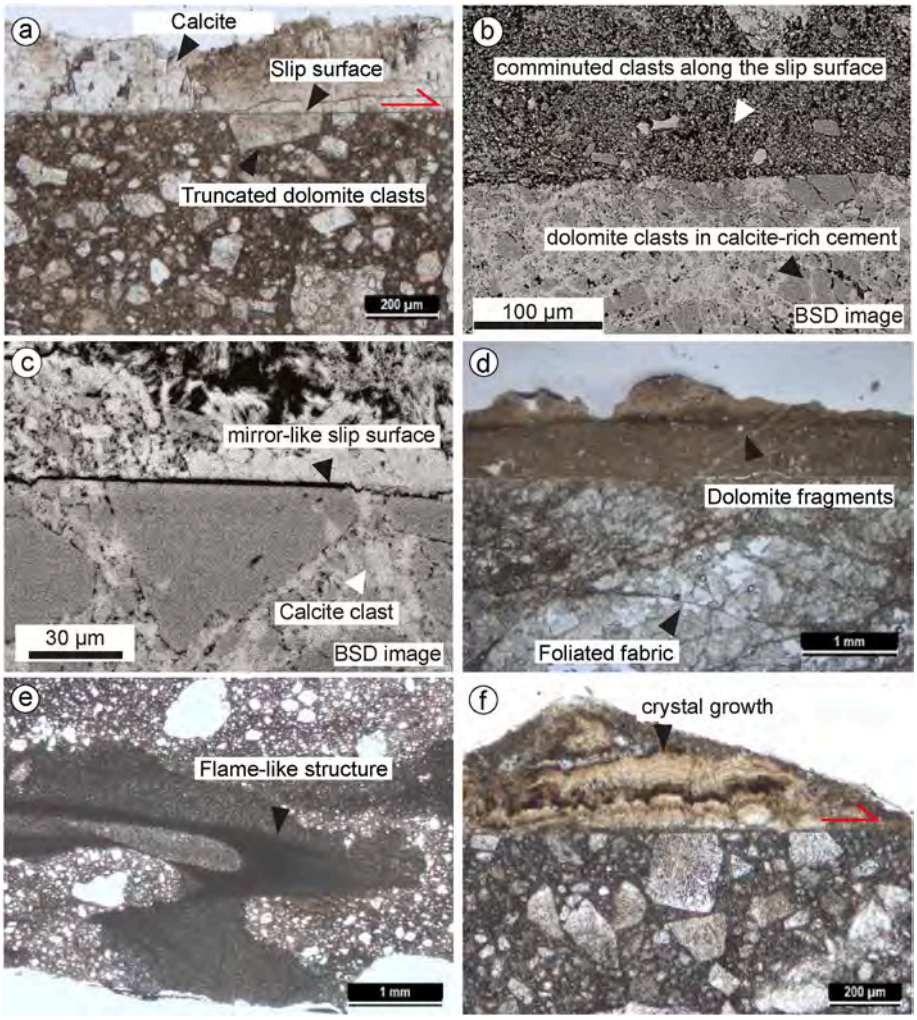

Fig. 10. Plane polarized (PPL) and SEM images showing textural characteristics of cohesive slip surfaces in the ultracataclastic and cataclastic domains. (a) Mirror-like localized slip surface with truncated dolostone clasts. (b) Calcite cementing dolostone survivor clasts along slip surfaces. (c) Detail of truncated dolostone clast and smaller calcite clasts of previous veins along slip surface, indicating cyclic fracturing. (d) Example of ultracomminution of dolostone in the mm-thick slip zone, surrounded by foliated cataclasite. (e) Flame-like structures within the ultracataclastic fault core. (f) Calcite crystals growing orthogonal to the slip surfaces (red arrow) with truncated clasts. BSD, back-scattered electron image.

On the other hand, mosaic breccias have a positively skewed frequency distribution, with *AR* values up to 8. Mean values ± 1σ of *AR* are 1.41 ± 0.29 for ultracataclasites, 1.49 ± 0.35 for cataclasites, and 2.34 ± 1.44 for breccias (Fig. 13a–c). The circularity values in ultracataclasites and cataclasites are generally >0.3, while mosaic breccias show minimum values also <0.3. Mean values ± 1σ of circularity are 0.73 ± 0.12 and 0.70 ± 0.13 for ultracataclasites and cataclasites, respectively; mosaic breccias has mean value of 0.53 ± 0.20. Overall, mosaic breccias have higher Aspect Ratio and lower Circularity values than ultracataclasites and cataclasites, in which clasts are generally equant and well rounded.

5. Discussion

5.1. Mosaic breccias and structural evolution of the Monte Marine fault

The poorly cohesive to loose mosaic breccias distributed along the MMF, developed in dolomitized massive to well-layered limestones, have the following key features:

1) they are systematically interposed between the cataclastic fault core and the fractured footwall damage zone (Figs. 3 and 7), thus forming a rather continuous body over the entire fault zone length;
2) their contact with the fault core rocks and the fractured damage zone is generally sharp, often marked by subsidiary faults, and locally transitional, but, in any case sub-parallel to the attitude of the principal fault surface (Figs. 3c and 7), suggesting that they are tectonic breccias associated with extensional faulting rather than with the compressional deformation phase;
3) at the mesoscale, they preserve folded and partially disrupted beds of the well-layered Corniola Formation, with still visible flattened, elongated bed-parallel chert nodules (Fig. 7a–c), which are progressively dragged toward the master fault surface. These features indicate that (i) the mosaic breccia is not a sedimentary breccia incorporated within, or smeared along, the extensional MMF, but an *in-situ* pervasively fragmented rock, and (ii) the mosaic breccias developed after a relevant normal drag of the Corniola Formation, and therefore brecciation did not occur during the embryonal or early stages of normal faulting;
4) they are generally poorly cohesive and, in places, completely loose (Fig. 8), indicating that renewed fracturing overprinted the sealing by calcite cements and suggesting a development during progressive exhumation from shallow crustal depth (<2–3 km) accompanied by cyclic reworking of the fabric;
5) they are affected by a pervasive mesh of extensional fractures from the sub-centimeter to micrometer scale (Fig. 7c and 8c), randomly

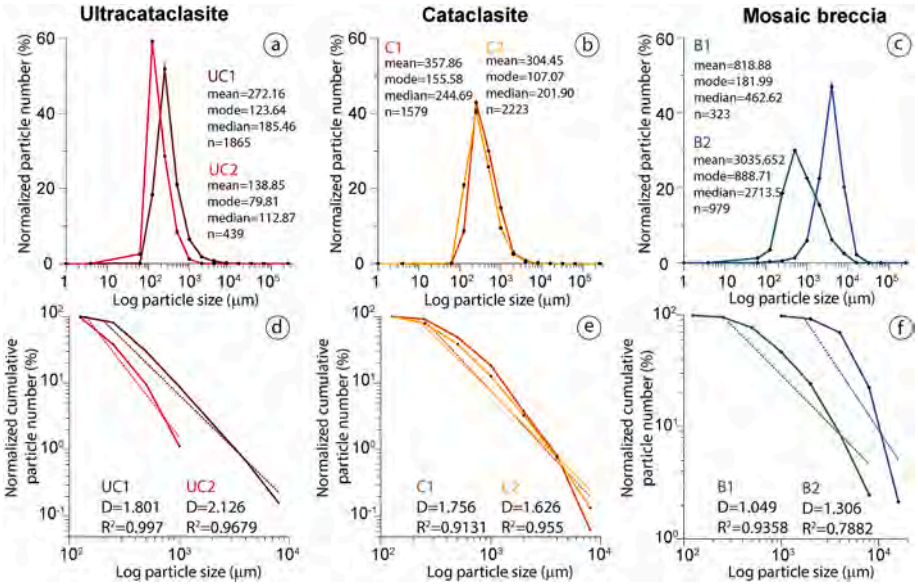

Fig. 11. Results of two-dimensional grain size distributions and fractal dimensions obtained via image analyses on cohesive samples. (a) Particle size distributions of ultracataclasites. (b) Particle size distributions of cataclasites. (c) Particle size distribution of mosaic breccias. (d) Fractal dimensions (D-values) of ultracataclasites. (e) Fractal dimensions (D-values) of cataclasites. (f) Fractal dimensions (D-values) of mosaic breccias.

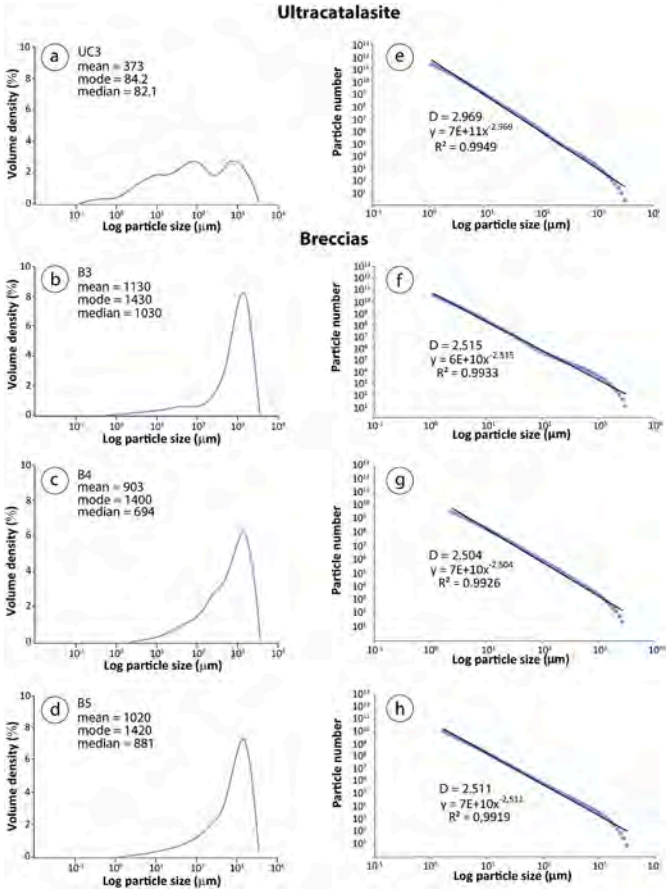

Fig. 12. Results of three-dimensional grain size distributions (a–d) and fractal dimensions (e–h) of a poorly cohesive ultracataclasite and three representative samples of loose mosaic breccias (via laser diffraction granulometry). Particle size distributions are shown in the left, and cumulative particle size distributions (fractal dimensions) are shown in the right column.

oriented or with local radial geometries, resulting in a micro-jigsaw texture and accommodating significant volumetric deformation and negligible shear strain.

6) they contain stretched and pervasively fragmented chert nodule that are locally sheared, offset and smeared along minor normal faults (Fig. 7e), indicating that brecciation is not a very last stage event (for example associated with intense weathering during exhumation) but is a syn-kinematic process imparted by fault activity. Such chert nodules are by far more fragmented than other chert nodules used as stress indicators in pelagic sequences in Central Apennines of Italy (Antonellini et al., 2020).

According to these field observations, a schematic structural evolution of the Monte Marine Fault can be summarized as in Fig. 14. In the early stage of faulting, the dolomitized and well-layered carbonates in the footwall are dragged toward the master fault, and an incipient cataclastic fault core surrounded by a fractured damage zone starts to form (Fig. 14a). Bed-perpendicular stylolites inherited from the previous compressive phase are also present within the damage zone. Some of the subvertical fractures can also be inherited from the Jurassic synrift normal faulting, although we exclude such contribution since subvertical dolomite veins were never observed in the footwall damage zones. With increasing fault displacement (Fig. 14b) cataclasis in the fault core proceeds and the bedding in the damage zone is further dragged toward the master fault surface. Chert nodules in the footwall damage zone are flattened due to local compression induced by fault movement (i.e., kinematic stress field with local σ1 forming 45° with respect to the master fault surface), and stretched in the direction parallel to bedding dip. Fracturing increases within the damage zone, and both fault core and damage zone widen. In the third stage (Fig. 14c) a mosaic breccia interposed between the fault core and the outer footwall damage zone develops producing intense fragmentation of the previous structural fabric. The origin of this breccia is discussed in the next section. Finally, further displacement is accommodated within the fault core that partially incorporates brecciated material (Fig. 14d). In this stage, the brecciated footwall material starts to behave as a poorly cohesive granular material made of angular clasts. The stretched and pervasively fragmented chert nodules are sheared and smeared along minor faults in the damage zone. Renewed fracturing and brecciation can occur repeatedly. This schematic evolutionary model indicates that

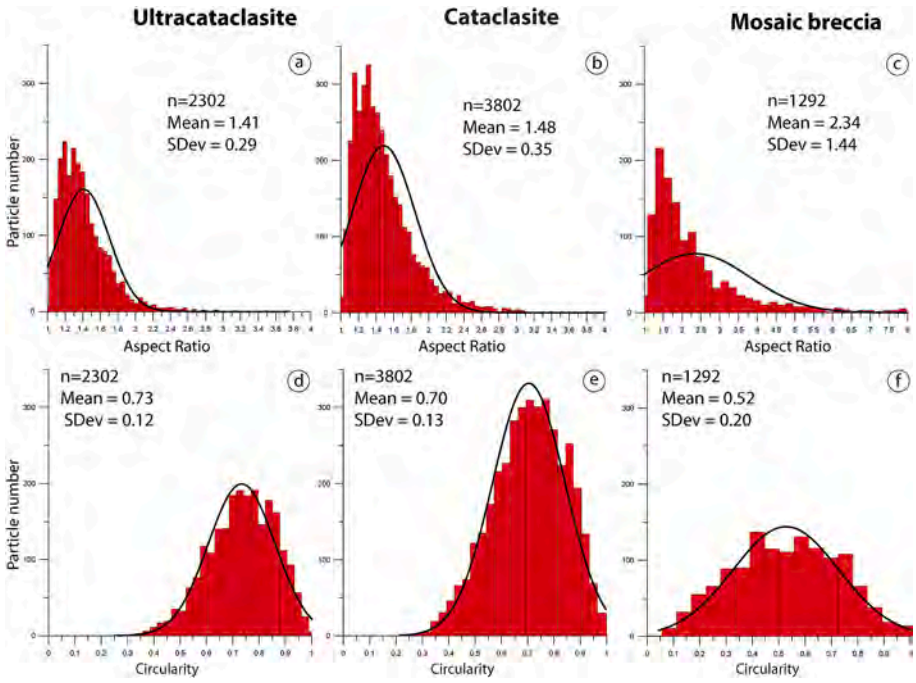

Fig. 13. Grain shape distribution data from ultracataclasites, cataclasites and mosaic breccias (via image analysis). (a–c) Aspect ratios of ultracataclasites, cataclasites and mosaic breccias, respectively. (d–f) Circularity of ultracataclasites, cataclasites and mosaic breccias.

mosaic breccias are not an embryonal product in the fault zone lifetime, but they postdate the relevant normal dragging and are associated with cyclic fracturing during exhumation from ~2 to 3 km to shallower depths.

5.2. Origin of mosaic breccias as in-situ shattered rocks

Based on the characteristics described above, the mosaic breccias along the MMF recall some of the meso-to micro-scopic features typical of shattered and pulverized rocks described along seismogenic fault zones (e.g., Brune, 2001; Dor et al., 2006; Rockwell et al., 2009; Mitchell et al., 2011). Pulverized rocks have been mainly, but not only, reported in strike-slip fault zones with an asymmetric distribution along strike and developed in tight crystalline protoliths (e.g., granitoids, gneisses; Dor et al., 2006; Rockwell et al., 2009; Mitchell et al., 2011; Muto et al., 2015; Williams et al., 2021; Ostermeijer et al., 2022). The mosaic breccias within the MMF footwall have larger particle sizes (mean particle size of 100s–3000 μm, Figs. 11–12) compared to the "classic" fine-grained pulverized rocks (mean particle size of 10s–100 s μm, e.g., Williams et al., 2021), but compare better with the lower-strain categories of "transitional-mixed", "fragmented-shattering", and only locally "gritty powder", recognized by Ostermeijer et al. (2022) by quantifying the heterogeneous fragmentation of granitoids along the San Andreas Fault. In a similar way, fracture intensity within the volumes of mosaic breccia in the MMF is highly heterogeneous in space, but the extreme silt-like grain sizes of pulverized granitoids are never attained.

Rock pulverization, and similarly to it, rock shattering over large volumes (up to 100s m away from the principal fault trace) have been interpreted to be genetically associated with dynamic loading during the propagation of multiple earthquake ruptures (Dor et al., 2010; Fondriest et al., 2015; Rowe and Griffith, 2015; Aben et al., 2017; Whearty et al., 2017). We suggest that the large volumes of mosaic breccias within the MMF footwall have a dynamic origin *lato sensu*, i.e. they are the cumulative result of deformation processes activated during large earthquakes rupturing the principal fault surface, or during the propagation of multiple mainshock-aftershock seismic sequences. In the following, we review the different mechanical models in the literature that have been proposed to explain coseismic rock shattering/pulverization based on field, experimental and numerical modelling constraints. We assess the compatibility of these models with the deformation intensity and spatial distribution of mosaic breccias along the MMF and discuss the feasibility of other earthquake-related generation mechanisms.

The shattering/pulverization mechanisms proposed in the literature mainly refer to mode II ruptures along strike-slip faults and include:

(1) Dynamic tensile loading: any approximately mode II earthquake rupture propagating unilaterally along a fault in a homogenous medium will produce dynamic compression on one side of the fault tip and transient dynamic tension on the opposite side (Griffith et al., 2009; Okubo et al., 2019). The magnitude of the tensile stresses and their orientation depend on the rupture parameters and mainly on its propagation speed (e.g., Poliakov et al., 2002; Di Toro et al., 2005; Griffith and Prakash, 2015). Dynamic rupture models combined with recent dynamic loading experiments indicate the potential of sub-shear ruptures to fragment the rocks in tension (i.e., transient tensile stresses larger than ~10 MPa) at relatively low strain rates of ~10^{-3} s^{-1} (Payne and Duan, 2017; Griffith et al., 2018; Smith and Griffith, 2022) up to 100s m distance from the propagating rupture tip. Such loading conditions would tend to generate anisotropic fracture networks which are not totally consistent with the isotropic fabric of pulverized rocks; in addition, the fragment sizes produced in dynamic tension experiments are systematically larger (i.e., lower fracture density) than those generated under compressive loading experiments (Barber and Griffith, 2017; Yao et al., 2020).

In the case of the MMF the shattered mosaic breccias are located in the footwall of the principal fault surface. Assuming that most of the large earthquake ruptures along this normal fault system would propagate from 7 to 10 km depth up-dip, as it was the case of recent $M_w > 6$ mainshocks in the region (Cirella et al., 2009; Chiaraluce et al., 2017), the footwall block would be systematically under dynamic compression (Ma, 2009). This implies that dynamic tensile loading is not a viable rock shattering mechanism unless we assume a statistically favored seismic rupture scenario in which the two overstepping fault segments rupture together. In addition, there is seismological evidence of dominant along strike rupture directivity for mainshock and aftershocks ($3.0 \leq Mw \leq 6.1$) towards SE (main faults striking NW-SE) in the L'Aquila 2009 seismic sequence (Calderoni et al., 2015). The L'Aquila seismic sequence

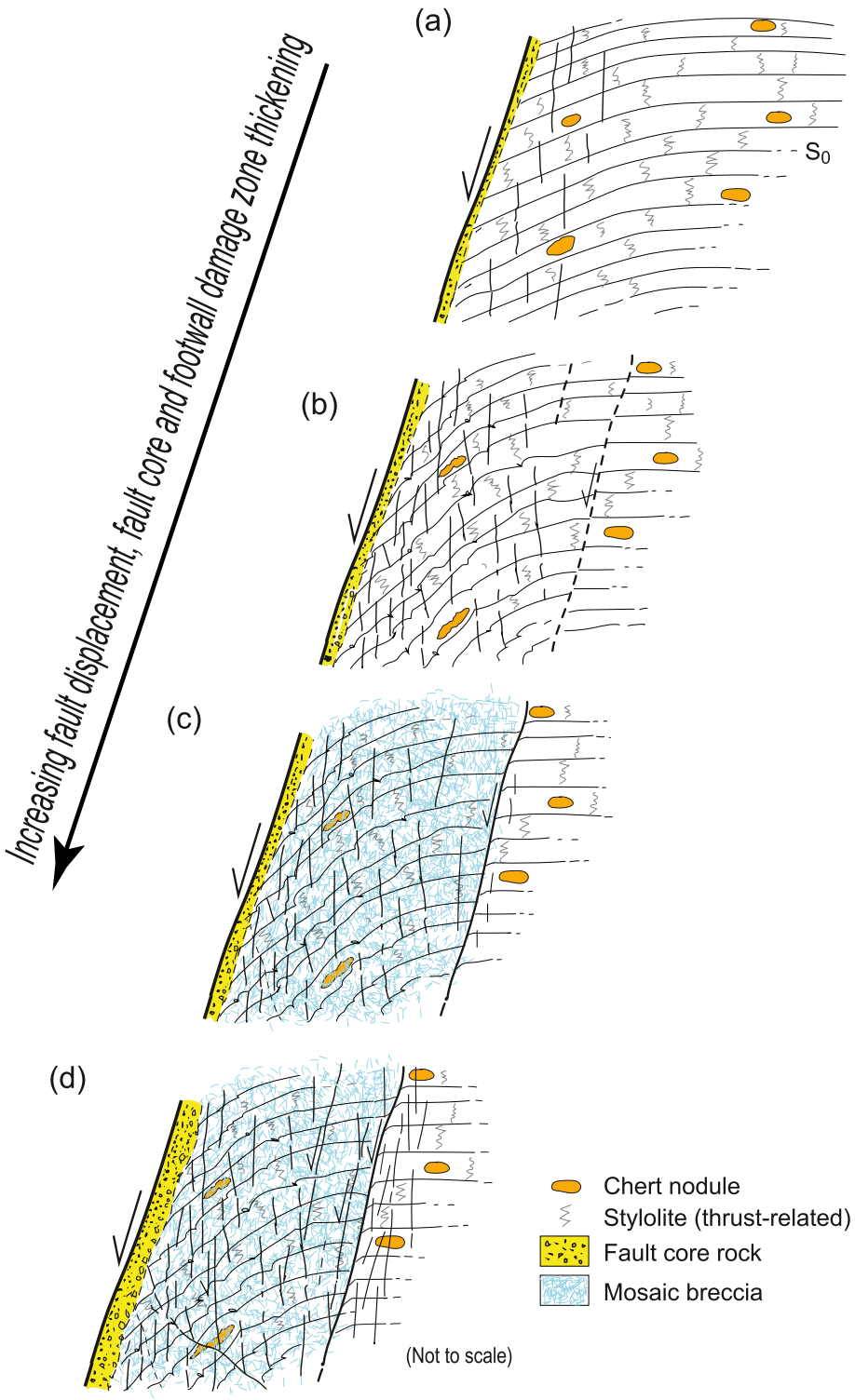

Fig. 14. Conceptual evolutionary model (not to scale) of the Monte Marine Fault showing the timing of breccia development. (a) Early faulting: cataclastic fault core and fractured damage zone start to form. (b) With increasing displacement the beds are further dragged toward the master fault surface, and fault core and damage zone increase in thickness. Chert nodules are stretched in the direction parallel to bedding dip. (c) Mosaic breccias develop overprinting the previous structural fabric (dragged and fractured dolomitized Corniola Formation), producing a severe fragmentation of the layered dolostone and flattened chert nodules. (d) Further displacement is accommodated within the cataclastic fault core and minor faults overprint the breccias. Ultracataclasites continue to form localized near the master fault surface, as well as along the minor faults in the footwall damage zone. The pervasively fragmented (pulverized) chert nodules are offset and smeared along minor normal faults. The brecciation may occur repeatedly to further reduce grain sizes down to ~0.1 mm.

was associated with a fault system located ~10–20 km to the SE (L'Aquila-Paganica area) and ~7–15 to the NE (Campotosto Lake area) of the MMF discussed here (Fig. 1a). However, the seismic ruptures that broke the MMF might have had a preferential NW rupture direction. Moreover, little is still known about the dynamic effects and stress-strain distribution related to the up-dip and concomitant along strike (i.e. mode II-III) earthquake rupture propagation in these extensional tectonic settings.

(2) Dynamic isotropic tensile loading: dynamic simulations of subshear earthquake ruptures propagating along a bimaterial fault interface with an elastic moduli contrast (e.g. 20%) have been shown to generate isotropic tensile pulses of 10–20 MPa in excess of confining pressure up to 100s m away from the principal fault surface. This "wrinkle-like" tensile pulse occurs on the stiffer side of the fault and deform the rocks at strain rates of $\sim 10^{-2}$ s^{-1} for durations of a few milliseconds (Ben-Zion and Shi, 2005; Payne and Duan, 2017; Xu and Ben-Zion, 2017) sufficient to induce dynamic fragmentation under volumetric tensile expansion. This represent a viable mechanism to explain the isotropic fracture pattern of pulverized rocks and their asymmetric distribution along seismogenic faults, since the bimaterial interface encourages sustained preferred rupture directivity (e.g., Xu and Ben-Zion, 2017). It has to be noted that likely other factors such as stress heterogeneity and geometric effects could potentially produce similar isotropic tensile pulses at certain distances from the seismogenic fault in absence of a bimaterial interface (e.g., Calderoni et al., 2015); however, to date, there are little constraints from numerical models on these rupture scenarios.

In the case of the MMF, the structural setting inferred from surface geology and the available subsurface information (Ghisetti and Vezzani, 1999; Buttinelli et al., 2018; Servizio Geologico d'Italia, 2010; Servizio Geologico d'Italia, 2022) is not consistent with the occurrence of a bimaterial interface at depth. This seems also the case of many extensional fault systems of the Central Apennines (Calderoni et al., 2015). Therefore, the model of isotropic tensile pulse related to a bimaterial fault interface cannot explain the origin of shattered mosaic breccias in the MMF.

(3) Fragmentation under dynamic compression: based on dynamic compression experiments, at high loading rates multiple fractures can propagate simultaneously before stress is relieved leading to rock fragmentation without shearing (i.e., shattering/pulverization). The strain rate threshold for rock shattering and pulverization in compression is $\geq 100\ s^{-1}$ for non-porous rocks under single loading and can be reduced up to 50% due to preexisting damage, to successive milder loadings, or to cyclic loading during a single earthquake (Doan and Gary, 2009; Doan and Billi, 2011; Doan and d'Hour, 2012; Aben et al., 2016; Fondriest et al., 2017; Braunagel and Griffith, 2019). In the case of subshear earthquake ruptures in a homogenous elastic medium, such large strain rates can be attained in the wall rock only at distances of few centimeters from the rupture tip and up to ~0.1 m under very favorable conditions, e.g., a combination of high rupture speed, fracture energy and number of previous seismic loadings (Aben et al., 2017). On the contrary, the propagation of stable supershear rupture fronts, seismologically and geodetically observed along major or plate boundary faults, has the potential to reach pulverization strain rate thresholds up to 100s m away from the fault surface (e.g., Bouchon and Vallée, 2003; Socquet et al., 2019; Bao et al., 2019). That said, the off-fault loading conditions associated with supershear ruptures are different from the one of dynamic compressive experiments (i.e., uniaxial P-wave loading), and therefore the characteristics of the dynamically induced fracture network (e.g., its geometry, anisotropy) are not easy to predict. Another important point is that dynamic shattering in compression also requires significant stresses, larger than the dynamic compressive strength of the rocks, at relatively shallow depths (<1–3 km). Large dynamic compressive stresses are easier to be attained in strike-slip or compressive tectonic settings compared to extensional ones, that are characterized by much lower mean stresses (Sibson, 1974).

In the case of the MMF, the volumes of *in-situ* shattered mosaic breccias are not compatible with a dynamic compression origin due to the propagation of multiple subshear earthquake ruptures in an elastic homogeneous medium. At the same time, the MMF and the seismogenic extensional fault systems of the Central Apennines are not associated with the propagation of stable supershear ruptures as observed along 100s km-long mature or plate boundary faults. However, this does not exclude that transient supershear rupture conditions can be attained when large earthquakes propagate within these more immature fault zones (see point 4 below for more details).

(4) Dynamic loading due to earthquake ruptures propagating in low-velocity zones: recent dynamic rupture models investigated the effect of a preexisting damage zone on the propagation of a new subshear earthquake rupture (e.g., Huang et al., 2014). These studies demonstrated that if the interface between the low-velocity damage zone and host rocks is sharp enough, the earthquake rupture will generate *fault zone waves* (i.e., reflected waves and head waves) which can influence the rupture dynamics and modulate properties such as rupture speed, slip rate, and rise time. In particular, head waves can cause large oscillations of rupture speeds with transient or even permanent transition to a supershear rupture. Moreover, the presence of a low-velocity damage zone (corresponding to the densely fractured rock volumes) causes a rotation of the background stress field that can induce dynamic permanent strain on both extensional and compressional sides of the fault tip (Huang et al., 2014). This implies that the conditions of dynamic rock fragmentation in compression could be attained within the fault zone transiently over significant distances from the rupture tip. Importantly, the simulations of Huang et al. (2014) are for a mode II ruptures on strike-slip faults in 2D. Therefore, the translation of these results to other tectonic settings or considering mode III rupture components is not trivial.

In the case of the MMF, the occurrence of a preexisting damage or inherited fault zone could have significantly contributed to the dynamic generation of the mosaic breccia volumes. Indeed, the fault zone is characterized by a complex internal structure, with structural units of contrasting elastic properties often separated by sharp boundary faults. In addition, the modelling of seismological data of the M_w 6.1 L'Aquila mainshock, which ruptured a nearby similar fault system, suggests that the rupture front transiently reached supershear rupture velocities during its up-dip propagation (Cirella et al., 2012). Another factor that has been poorly investigated in dynamic loading experiments is the effect of pore fluid pressure. Indeed, under compressive loading and fluid saturated conditions rock shattering might have occurred at significantly lower undrained effective stresses (e.g., Renard et al., 2023). On the other side, it has to be noted that the shallow extensional tectonic setting of the MMF was likely characterized by low background mean stresses (i.e., it is more difficult to fracture in compression) and that in the Huang et al. (2014) simulations most of the off-fault strain will still occur in the tensile side of the fault rupture tip.

(5) Dynamic decompression and hydrofracturing: based on experiments of instantaneous decompression of gas saturated rock samples, Mitchell et al. (2013) suggested that this could be a viable mechanism to progressively shatter or pulverize low-porosity rocks during earthquake rupture propagation. According to this model, rock fragmentation occurs through a sudden volumetric expansion driven by pore fluid (i.e., hydrofracturing) since the confining pressure dropped faster than the pore pressure in the rock. This hydrofracturing mechanism can potentially occur both with gas (Mitchell et al., 2011; Hesse et al., 2022) and liquids (e.g., pore water). Based on the above, rock shattering/pulverization can be associated with dynamic tensile loading, with isotropic tension due to bimaterial fault interfaces, with large coseismic stress drops at shallow depth, or to the dynamic opening of fault jogs and wall rock implosion. The rock shattering or pulverization will occur at the length scale at which the induced transient pore fluid overpressure is released, which can also be very local (e.g., Billi et al., 2023).

In the case of the MMF, rapid dynamic decompression can be a mechanism locally activated off-fault both during the propagation of

mainshock earthquake ruptures and of aftershock sequences within the fault zone. Indeed, in this extensional tectonic setting, a close to isotropic tensile effective stress state might be relatively common at shallow depths (<1–3 km), considering the low compressive stress state and hydrostatic pore fluid pressure. Consequently, with reasonably high dynamic stress drops (10–40 MPa) as the ones estimated for recently ruptured fault systems in the region (M_w 6.1 2009 L'Aquila mainshock; Cocco et al., 2016) and/or stress perturbations near fault intersections, large off-fault rock volumes could transiently be under dynamic tension. Considering the scale invariance of seismic stress drops (Cocco et al., 2016), this would happen not only off-fault of the large earthquake ruptures, but also on a longer term due to the propagation of aftershock sequences which entirely saturate large volumes around the principal fault surfaces (e.g., Valoroso et al., 2013, 2014; Fondriest et al., 2020).

6) Fragmentation in tension due to dynamic pore pressure waves: recent numerical simulations of subshear mode I dynamic fracture propagation in a fluid saturated elastic medium showed the generation of pore pressure waves up to few MPa potentially able to fracture the rocks in tension (Ni et al., 2021). In addition, the complex interaction between mechanical waves and pore pressure waves can result in an increase of the fracture tip propagation velocity up to supershear also due to the generation and merging with fore-running "daughter" ruptures (Ni et al., 2021). This appealing mechanical model has only been tested for mode I ruptures while future investigations are needed to assess the occurrence of similar processes for modes II and III ruptures.

In the case of the MMF, rock fragmentation due to pore pressure waves would represent an elegant and effective way to explain the genesis of large volumes of *in-situ* shattered mosaic breccias in an extensional setting at shallow depth (<1–3 km) and hydrostatic pore fluid pressure. However, this explanation still lacks scientific support.

In more general terms, the textural difference between the dolomitic shattered mosaic breccias of the MMF and the fine-grained pulverized granitoids could derive from a lithological effect. Accordingly, recent experimental studies seem to suggest that the asymmetric distribution of pulverized rocks along seismogenic faults might not be only explained as the result of preferred rupture directivity (e.g., Dor et al., 2006). Indeed, different lithologies loaded under comparable dynamic conditions result in distinct fracture types and density (e.g., Aben et al., 2017; Smith and Griffith, 2022), because at the microscale the dynamic growth of fractures is controlled by material dependent properties such as fracture toughness and stress perturbation effects related to rock microstructure (e.g., Smith and Griffith, 2022). At the same time, it is worth to keep in mind that a direct comparison between the experimentally deformed rocks and the natural shattered/pulverized rocks at the field scale is intrinsically biased (Xu and Ben Zion, 2017), since both rock strength as well as elastic moduli are strongly scale-dependent properties.

Based on our observations, we conclude that the shattered mosaic breccias along the MMF are the result of several seismic cycles, but are mainly produced coseismically during the propagation of multiple large earthquake ruptures (i.e., Mw 6–7 earthquakes rupturing large parts or the whole fault system) and the following aftershock sequences which activate large volumes around the principal fault surfaces for several months after the main earthquake ruptures. No single preferred scenario among the six presented above can be chosen to explain the origin of mosaic breccias, but the most compatible are dynamic decompression and hydrofracturing due to mainshock and/or aftershock sequences, the important potential role of dynamic pore pressure waves, the dynamic effects of preexisting low-velocity damage zones, and dynamic tensile loading conditions due to the concurrent rupture of overstepped fault segments at shallow depth, a common rupture scenario for the extensional faults of the Central Apennines. In this context, we believe that until simulations of realistically complex rupture fronts are carried out in 3D, for extensional faults, with modelling of dynamic fracturing, any of the above scenarios cannot be ruled out a priori.

On the other hand, it is difficult to explain the formation of the shattered breccias in a purely quasi-static scenario, considering that these rocks are affected by extreme fracture densities over large distances (up to few 100s m) compared to "classic" damage zones. Dolomitic breccias with similar characteristics have been described by Frost et al. (2009) along the Salzach-Ennstal-Mariazell-Puchberg (SEMP) strike-slip fault system in the Eastern Alps. Here, the authors reported up to ~50 m of intensely fragmented dolomitic breccias surrounding a ~10 m-thick cataclastic fault core, while limestones in the other side of the fault are affected by low fracture density. In their conceptual model, Frost et al. (2009) consider the breccia volumes to be formed by progressive quasi-static fracturing during the embryonal or early stages of faulting and then being progressively consumed during strain localization within the fault core. More recently other authors alternatively concluded that these dolomitic breccias with asymmetric distribution were likely recording several cycles of coseismic dynamic fracturing along the SEMP (Schröckenfuchs et al., 2015). The case study of the MMF is not strictly comparable with that of the SEMP, since the latter is 400 km-long fault with cumulative displacement of 60 km and the breccias exhumed from 4 to 6 km depth, while the MMF outcrops were exhumed from <2 km depth along a ~12 km-long fault system with a maximum of 1.5 km of displacement. More importantly, the shattered mosaic breccias along the MMF were not exclusively produced during the early stages of faulting since they both show evidence of cyclic fracturing and sealing, and postdate the normal dragging of the Corniola Formation in the footwall block (Fig. 14).

5.3. Factors controlling along-strike variation of in-situ shattered rocks

The *in-situ* shattered breccias associated with the MMF have different along-strike thicknesses, ranging from a minimum of ~30 m in the NW sector (Barete, Fig. 2a and 3), up to ~500 m in the central sector near Pizzoli village (Fig. 2a, 4–5). In the latter, NW-SE-trending extensional fault segments are connected by an E-W-trending fault segment and cut through older thrust faults. Such geometrical features suggest that several factors may have contributed, during the growth history of the MMF, to develop the observed greater volumes of mosaic breccias in the central sector (Fig. 15). These are:

1) the presence of pre-existing thrust-related fractures in the host rock, providing inherited damage before normal faulting (Fig. 15a). In the theoretical framework of a dynamic *lato sensu* origin for the *in-situ* shattered mosaic breccias, the occurrence of preexisting damage associated with older compressional deformations can explain the larger extent of rock shattering in the SE fault zone sector (see point 4 of section 5.1). In addition, also the effect of initial rock damage at the microscale has been experimentally proven to significantly lower both the strain rate and stress thresholds for rock shattering and pulverization (Doan and d'Hour, 2012; Aben et al., 2016; Smith and Griffith, 2022). Therefore, pre-damaged rocks would be preferentially shattered since heterogeneous damage distribution generates a positive feedback loop promoting further fragmentation in these rocks (Ostermeijer et al., 2022);
2) fracture density increases at the tip process zones (McGrath and Davison, 1995; Kim et al., 2004; Berio et al., 2023) of the two NW-trending segments, before E-W hard-linkage faulting (Fig. 15b);
3) the fault intersection and mechanical interaction between low-angle thrust faults still preserved in the footwall of the Monte Marine Fault and subsidiary high-angle extensional faults (Fig. 15c–e g., Leah et al., 2018; Lucca et al., 2019);
4) the generation of *fault zone waves* (reflected and head waves) due to seismic ruptures propagating within already damaged and brecciated rock volumes interposed between the two overlapping NW-trending fault segments might have led to transient supershear ruptures favoring further rock shattering (see point 4 of section 5.2; Huang et al., 2014).
5) the concurrent rupture of the two overlapping NW-trending fault segments would produce dynamic tensile pulses in the overstepping

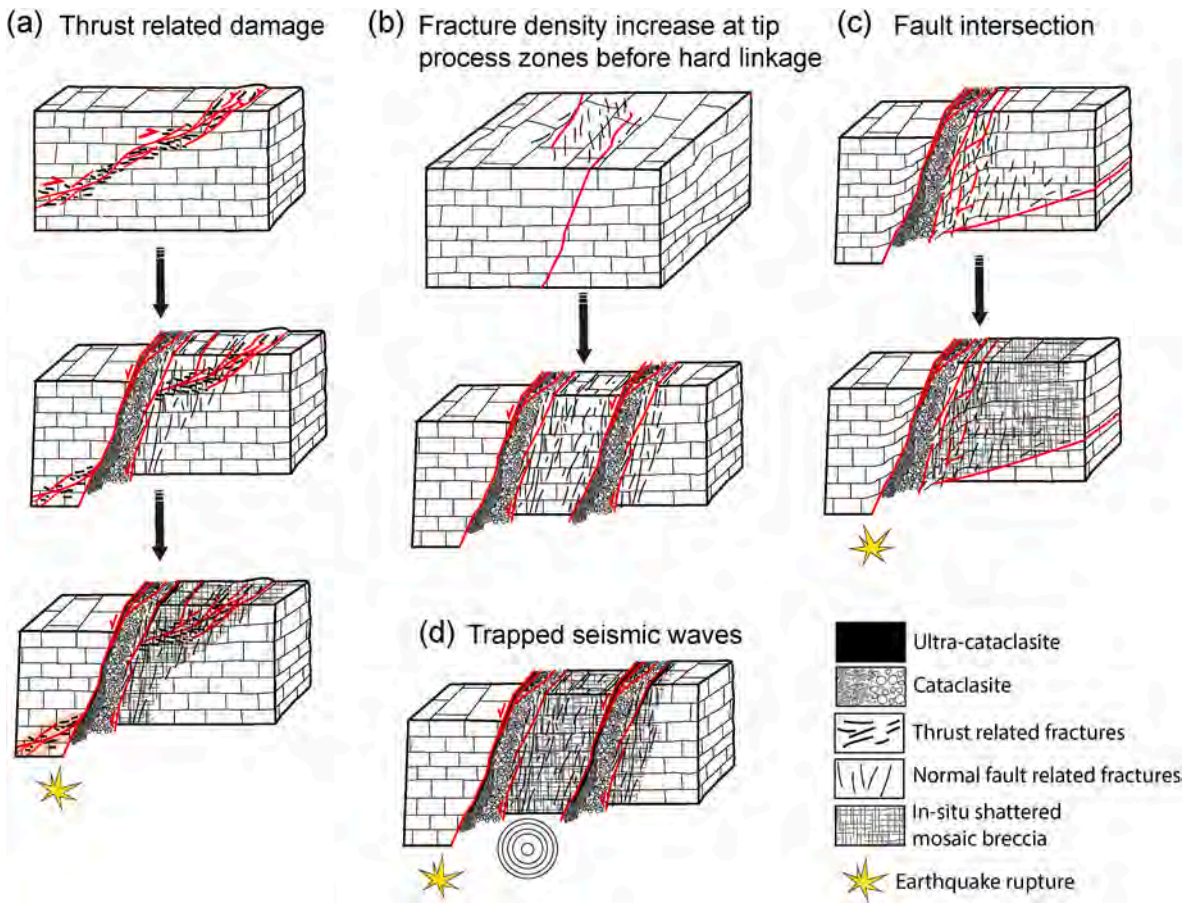

Fig. 15. Proposed 3D-block diagrams showing geometrical factors concurring to the development of different volumes of *in-situ* shattered mosaic breccias along the Monte Marine Fault. (a) Thrust-related inherited damage. (b) Fracture density increase at the tip process zones in the overstep region before hard-linkage of NW-trending normal fault segments. (c) Mechanical interaction and fault intersection between low-angle thrust fault and high-angle extensional faulting. (d) Trapped seismic waves between overlapping extensional faults.

region and determine dynamic shattering in tension or due to hydrofracturing (see section 5.1).

5.4. Strain localization along the MMF

Several lines of evidence indicate that the fault core rocks of the MMF developed partially at the expenses of *in-situ* shattered mosaic breccias. The boundary between the footwall shattered breccias and the fault core cataclasites is generally sharp (secondary faults, Fig. 7b) but locally transitional and marked by a progressive decrease in grain size and the disruption of jigsaw breccia texture. Ultracataclasites and cataclasites in the fault core are markedly different from adjacent *in-situ* shattered mosaic breccias in terms of particle size distribution, fractal dimension and clast shape parameters (Figs. 11–13). At the same time, the slip zones of the former show meso-to micro-scale evidence of normal fault dragging and shearing on marly interlayers, rotation of centimeter-sized clasts within ultra-comminuted matrix, foliation in mixed calcite-dolomite cataclasites, cyclic fracturing, comminution and cementation (Fig. 10c). These features are consistent with shear strain localization within the fault core and reworking *in-situ* shattered mosaic breccias. This interpretation is also supported by particle size distributions and particle shape data. Indeed, the fractal dimension increases from the *in-situ* shattered mosaic breccias ($D = 1$–1.3 in two-dimensions and ~2.5 in three-dimensions) towards the cataclasites ($D = 1.6$–1.7 in 2D) and ultracataclasites ($D = 1.8$–2.1 in 2D and ~2.9 in 3D), consistently with the activation of shear strain localization mechanisms with flaking during interparticle rolling, and grinding, which promote the increase in small particles and fractal value (Storti et al., 2003; Di Toro et al., 2005; Keulen et al., 2007). Similarly, particles Aspect Ratio decreases and Circularity increases from the *in-situ* shattered mosaic breccias to the cataclasites and ultracataclasites (Fig. 11), consistently with a greater comminution intensity and grain flaking approaching the master fault surface. Lastly, the occurrence of extremely localized slip zones bounded or truncated by smooth and mirror-like slip surfaces records extreme strain localization but cannot be unequivocally associated with fast coseismic or slow aseismic fault slip behavior (Delle Piane et al., 2017; Chinello et al., 2023). Indeed, mirror-like slip surfaces in carbonate gouges have been produced in experiments performed both at seismic and sub-seismic slip rates (1–10 μm/s to ~1 m/s; Fondriest et al., 2013; Verberne et al., 2014; Passelègue et al., 2019). In addition, the development of localized mixed calcite-dolomite foliations and the occurrence of variably comminuted rock layers with convolute geometries have been explained as consequence of contrasted mechanical behaviors, liquefaction and local fluid pressurization that can be related both to seismic and aseismic deformation (Niemeijer and Spiers, 2006; Faulkner et al., 2010; Smith et al., 2011, Smith et al., 2017).

6. Conclusions

The Monte Marine Fault is a seismogenic extensional fault segment belonging to the Upper Aterno River Valley Fault System in the Central Apennines, capable of earthquake ruptures with Mw up to ~7. Results from our field and laboratory analyses can be summarized as follow:

1) the footwall of the MMF, developed in massive and layered Jurassic dolostones, is characterized by a cross-sectional structure composed

of m-thick ultracataclasites and cataclasites, and large volumes (≥30 m thick) of *in-situ* loose shattered mosaic breccias interposed between the cataclastic fault core and the fractured damage zone;
2) the MMF consists of two NW-trending normal fault segments connected by an E-W breaching fault in an overstep sector, where the shattered breccias have greater width (up to ~500 m);
3) overall, the loose mosaic breccias have mean clast diameters of ~1–10 mm and fractal dimension value of D~2.5, lower than cataclasites (D~2.7–3) and other pulverized rocks in gneiss and granitoids (D~3) along active strike-slip faults. This could be related to a lithological effects associated with dynamic fracturing which should be further investigated experimentally;
4) the *in-situ* shattered mosaic breccias have a mostly isotropic fragmented texture with negligible shear strain and are suggested to have a dynamic origin *lato sensu*, i.e., they are the cumulative result of deformation processes activated during large earthquakes (mainshocks) rupturing the principal fault surface, or during the evolution of multiple mainshock-aftershock seismic sequences;
5) along-fault strike variations in the thickness of *in-situ* shattered mosaic breccia seem less dependent on rock composition and, instead, likely depend on geometrical and structural factors that acted during the evolution and growth of the MMF. In particular, the following factors may have contributed to produce larger volumes of shattered breccias in an overstep fault region: (i) the presence of inherited thrust-related fractures; (ii) the mechanical interaction between normal fault segments and thrust faults, (iii) the presence of higher fracture densities at the tip of normal fault segments before hard-linkage of NW-trending fault segments; (iv) dynamic effects of *fault zone waves* in the damaged rocks (likely compliant and low velocity materials) within the structurally complex overstep sector, and (v) transient tensile loading and shattering produced at the overstepping region due to the concurrent rupture of the two NW-trending principal fault segments.

CRediT authorship contribution statement

S. Cortinovis: Data curation, Formal analysis, Investigation, Writing – original draft. **M. Fondriest:** Conceptualization, Formal analysis, Funding acquisition, Writing – original draft, Writing – review & editing. **F. Balsamo:** Conceptualization, Formal analysis, Funding acquisition, Investigation, Supervision, Writing – original draft, Writing – review & editing. **A. Lucca:** Data curation, Formal analysis, Investigation, Writing – review & editing. **F. La Valle:** Data curation, Formal analysis, Investigation. **M. Pizzati:** Data curation, Formal analysis, Investigation, Writing – review & editing. **F. Storti:** Conceptualization, Supervision, Writing – original draft, Writing – review & editing. **G. Di Toro:** Conceptualization, Funding acquisition, Project administration, Writing – original draft, Writing – review & editing.

Declaration of competing interest

The authors declare the following financial interests/personal relationships which may be considered as potential competing interests: Giulio Di Toro reports financial support was provided by European Research Council. Michele Fondriest reports financial support was provided by EU-H2020.

Data availability

Data will be made available on request.

Acknowledgements

SC PhD program was supported by the 32° Cycle in Earth Sciences at the University of Parma, Italy. **GDT**, **FLV** and **MF** were funded by the ERC CoG project 614705 NOFEAR. **MF** was funded by EU-H2020 MSCA grant agreement N∘ 839880 (DAMAGE), NextGenerationEU and by the 2021 STARS Grants@Unipd programme. This work has also benefited from the equipment and framework of the COMP-HUB Initiative, funded by the 'Departments of Excellence' program of the Italian Ministry for Education, University and Research (MIUR, 2018–2022). Two anonymous reviewers are kindly thanked for their helpful comments and criticism which greatly improved the final version of this paper.

Appendix A. Supplementary data

Supplementary data to this article can be found online at https://doi.org/10.1016/j.jsg.2024.105144.

References

Aben, F.M., Doan, M.L., Mitchell, T.M., Toussaint, R., Reuschlé, T., Fondriest, M., Gratier, J.P., Renard, F., 2016. Dynamic fracturing by successive coseismic loadings leads to pulverization in active fault zones. J. Geophys. Res. Solid Earth 121 (4), 2338–2360.

Aben, F.M., Doan, M.L., Gratier, J.P., Renard, F., 2017. Coseismic damage generation and pulverization in fault zones: insights from dynamic Split-Hopkinson Pressure Bar experiments in Thomas, M.Y. In: Mitchell, T.M., Bhat, H.S. (Eds.), Fault Zone Dynamic Processes: Evolution of Fault Properties during Seismic Rupture, vol. 227. American Geophysical Union, Geophysical Monograph, pp. 47–80.

Agosta, F., Aydin, A., 2006. Architecture and deformation mechanism of a basin-bounding normal fault in Mesozoic platform carbonates, central Italy. J. Struct. Geol. 28 (8), 1445–1467.

Antonellini, M., Del Sole, L., Mollema, P.N., 2020. Chert nodules in pelagic limestones as paleo-stress indicators: a 3D geomechanical analysis. J. Struct. Geol. 132, 103979.

Balsamo, F., Storti, F., 2011. Size-dependent comminution, tectonic mixing, and sealing behavior of a structurally oversimplified"fault zone in poorly lithified sands: evidence for a coseismic rupture? Geol. Soc. Am. Bull. 123 (3–4), 601–619.

Balsamo, F., Clemenzi, L., Storti, F., Solum, J., Taberner, C., 2019. Tectonic control on vein attributes and deformation intensity in fault damage zones affecting Natih platform carbonates, Jabal Qusaybah, North Oman. J. Struct. Geol. 122, 38–57.

Bao, X., Zhang, M.H., Zhai, C.H., 2019. Fragility analysis of a containment structure under far-fault and near-fault seismic sequences considering post-mainshock damage states. Eng. Struct. 198, 109511.

Ben-Zion, Y., Shi, Z., 2005. Dynamic rupture on a material interface with spontaneous generation of plastic strain in the bulk. Earth Planet Sci. Lett. 236 (1–2), 486–496.

Barber, T., Griffith, W.A., 2017. Experimental constraints on dynamic fragmentation as a dissipative process during seismic slip. Phil. Trans. Roy. Soc. A: Math. Phys. Eng. Sci. 375, 20160002.

Berio, L.R., Balsamo, F., Pizzati, M., Storti, F., Curzi, M., Viola, G., 2023. Along-and across-strike variation of damage zone parameters in the Kornos-Aghios Ioannis normal fault, Lemnos Island, Greece. J. Struct. Geol. 177, 104981.

Billi, A., Storti, F., 2004. Fractal distribution of particle size in carbonate cataclastic rocks from the core of a regional strike-slip fault zone. Tectonophysics 384 (1–4), 115–128.

Billi, A., Smeraglia, L., Aldega, L., Balsamo, F., Barberio, M.D., Boschi, C., Caracausi, A., Carminati, E., Iannace, A., Mercuri, M., Pizzati, M., Tavani, S., 2023. Dolostone pulverization induced by coseismic rapid decompression of CO_2-rich gas in nature (Matese, Apennines, Italy). Earth Planet Sci. Lett. 604, 117996.

Blenkinsop, T.G., 1991. Cataclasis and processes of particle size reduction. Pure Appl. Geophys. 136, 59–86.

Blumetti, A.M., 1995. Neotectonic investigations and evidence of paleoseismicity in the epicentral area of the January–February 1703, Central Italy, earthquakes. Perspectives in Paleoseismol. 6, 83–100.

Boccaletti, M., Elter, P., Guazzone, G., 1971. Plate tectonic models for the development of the western Alps and northern Apennines. Nat. Phys. Sci. (Lond.) 234, 108–111. https://doi.org/10.1038/physci234108a0.

Bouchon, M., Vallée, M., 2003. Observation of long supershear rupture during the magnitude 8.1 Kunlunshan earthquake. Science 301 (5634), 824–826.

Braunagel, M.J., Griffith, W.A., 2019. The effect of dynamic stress cycling on the compressive strength of rocks. Geophys. Res. Lett. 46 (12), 6479–6486.

Brune, J.N., 2001. Fault normal dynamic loading and unloading: an explanation for "non-gouge" rock powder and lack of fault-parallel shear bands along the San Andreas fault. Eos Trans. AGU 82.

Buttinelli, M., Pezzo, G., Valoroso, L., De Gori, P., Chiarabba, C., 2018. Tectonics inversions, fault segmentation, and triggering mechanisms in the central Apennines normal fault system: insights from high-resolution velocity models. Tectonics 37 (11), 4135–4149.

Caine, J.S., Evans, J.P., Forster, C.B., 1996. Fault zone architecture and permeability structure. Geology 24 (11), 1025–1028.

Calamita, F., Pizzi, A., 1992. Tettonica quaternaria nella dorsale appenninica umbro-marchigiana e bacini intrappenninici associati. Studi Geol. Camerti 1, 17–25.

Calderoni, G., Rovelli, A., Ben-Zion, Y., Di Giovambattista, R., 2015. Along-strike rupture directivity of earthquakes of the 2009 L'Aquila, central Italy, seismic sequence. Geophys. J. Int. 203 (1), 399–415.

Carminati, E., Doglioni, C., 2012. Alps vs. Apennines: the paradigm of a tectonically asymmetric Earth. Earth Sci. Rev. 112 (1–2), 67–96.

Carminati, E., Doglioni, C., Scrocca, D., 2004. Alps vs Apennines. Special Volume of the Italian Geol. Soc. the IGC 32, 141–151.
Cello, G., Mazzoli, S., Tondi, E., Turco, E., 1997. Active tectonics in the central Apennines and possible implications for seismic hazard analysis in peninsular Italy. Tectonophysics 272 (1), 43–68.
Chiaraluce, L., Valoroso, L., Piccinini, D., Di Stefano, R., De Gori, P., 2011. The anatomy of the 2009 L'Aquila normal fault system (central Italy) imaged by high resolution foreshock and aftershock locations. J. Geophys. Res. Solid Earth 116 (B12).
Chiaraluce, L., Di Stefano, R., Tinti, E., Scognamiglio, L., Michele, M., Cattaneo Casarotti, M., De Gori, P., et al., 2017. The 2016 Central Italy seismic sequence: a first look at the mainshocks, aftershocks, and source models. Seismol Res. Lett. 88 (3), 1.
Chinello, M., Bersan, E., Fondriest, M., Tesei, T., Gomila, R., Di Toro, G., 2023. Seismic Cycle in Bituminous Dolostones (Monte Camicia Thrust Zone, Central Apennines, Italy). Geochemistry, Geophysics, Geosystems 24 (12), e2023GC011063.
Choi, J.H., Edwards, P., Ko, K., Kim, Y.S., 2016. Definition and classification of fault damage zones: a review and a new methodological approach. Earth Sci. Rev. 152, 70–87.
Cilona, A., Solum, J.G., Lucca, A., Storti, F., Balsamo, F., Taberner, C., 2019. Evolution of pore types and petrophysical properties of fault rocks in low-porosity carbonates. J. Sediment. Res. 18 (2), 94–107.
Cirella, A., Piatanesi, A., Cocco, M., Tinti, E., Scognamiglio, L., Michelini, A., Lomax, A., Boschi, E., 2009. Rupture history of the 2009 L'Aquila (Italy) earthquake from non-linear joint inversion of strong motion and GPS data. Geophys. Res. Lett. 36 (19).
Cirella, A., Piatanesi, A., Tinti, E., Chini, E., Cocco, M., 2012. Complexity of the rupture process during the 2009 L'Aquila, Italy, earthquake. Geophys. J. Int. 190 (1), 607–621.
Clemenzi, L., Storti, F., Balsamo, F., Molli, G., Ellam, R., Muchez, P., Swennen, R., 2015. Fluid pressure cycles, variations in permeability and weakening mechanisms along low-angle normal faults: the tellaro detachment. Geol. Soc. Am. Bull., Italy 127, 1689–1710. https://doi.org/10.1130/B31203.1.
Cocco, M., Tinti, E., Cirella, A., 2016. On the scale dependence of earthquake stress drop. J. Seismol. 20 (4) https://doi.org/10.1007/s10950-016-9594-4.
Cosentino, D., Asti, R., Nocentini, M., Gliozzi, E., Kotsakis, T., Mattei, M., et al., 2017. New insights into the onset and evolution of the central Apennine extensional intermontane basins based on the tectonically active L'Aquila Basin (central Italy). GSA Bulletin 129 (9–10), 1314–1336.
Delle Piane, C., Clennell, M.B., Keller, J.V., Giwelli, A., Luzin, V., 2017. Carbonate hosted fault rocks: a review of structural and microstructural characteristic with implications for seismicity in the upper crust. J. Struct. Geol. 103, 17–36.
Demurtas, M., Fondriest, M., Balsamo, F., Clemenzi, L., Storti, F., Bistacchi, A., Di Toro, G., 2016. Structure of a normal seismogenic fault zone in carbonates: the Vado di Corno Fault, Campo Imperatore, Central Apennines (Italy). J. Struct. Geol. 90, 185–206.
Di Toro, G., Nielsen, S., Pennacchioni, G., 2005. Earthquake rupture dynamics frozen in exhumed ancient faults. Nature 436 (7053), 1009–1012.
Doan, M.L., Billi, A., 2011. High strain rate damage of Carrara marble. Geophys. Res. Lett. 38 (19), 1–6.
Doan, M.L., d'Hour, V., 2012. Effect of initial damage on rock pulverization along faults. J. Struct. Geol. 45, 113–124.
Doan, M.L., Gary, G., 2009. Rock pulverization at high strain rate near the San Andreas fault. Nat. Geosci. 2 (10), 709–712.
Doglioni, C., 1991. A proposal for the kinematic modelling of W-dipping subductions-possible applications to the Tyrrhenian-Apennines system. Terra. Nova 3 (4), 423–434.
Dor, O., Ben-Zion, Y., Rockwell, T.K., Brune, J., 2006. Pulverized rocks in the Mojave section of the san Andreas Fault Zone. Earth Planet Sci. Lett. 245 (3–4), 642–654.
Dor, O., Chester, J.S., Ben-Zion, Y., Brune, J.N., Rockwell, T.K., 2010. Characterization of damage in sandstones along the Mojave section of the San Andreas Fault: implications for the shallow extent of damage generation. Mechanics, Struct. Evolution of Fault Zones 1747–1773.
Falcucci, E., Gori, S., Moro, M., Fubelli, G., Saroli, M., Chiarabba, C., Galadini, F., 2015. Deep reaching versus vertically restricted Quaternary normal faults: implications on seismic potential assessment in tectonically active regions: lessons from the middle Aterno valley fault system, central Italy. Tectonophysics 651, 186–198.
Falcucci, E., Gori, S., Bignami, C., Pietrantonio, G., Melini, D., Moro, M., Saroli, M., Galadini, F., 2018. The Campotosto seismic gap in between the 2009 and 2016–2017 seismic sequences of central Italy and the role of inherited lithospheric faults in regional seismotectonic settings. Tectonics 37 (8), 2425–2445.
Faulkner, D.R., Jackson, C A.L., Lunn, R.J., Schlische, R.W., Shipton, Z.K., Wibberley, C. A.J., Withjack, 2010. A review of recent developments concerning the structure, mechanics and fluid flow properties of fault zones. J. Struct. Geol. 32 (11), 1557–1575.
Ferrarini, F., Lavecchia, G., De Nardis, R., Brozzetti, F., 2015. Fault geometry and active stress from earthquakes and field geology data analysis: the Colfiorito 1997 and L'Aquila 2009 Cases (Central Italy). Pure Appl. Geophys. 172, 1079–1103.
Ferraro, F., Grieco, D.S., Agosta, F., Prosser, G., 2018. Space-time evolution of cataclasis in carbonate fault zones. J. Struct. Geol. 110, 45–64.
Fondriest, M., Smith, S.A.F., Candela, T., Nielsen, S.B., Mair, K., Di Toro, G., 2013. Mirror-like faults and power dissipation during earthquakes. Geology 41 (11), 1175–1178.
Fondriest, M., Aretusini, S., Di Toro, G., Smith, S.A.F., 2015. Fracturing and rock pulverization along an exhumed seismogenic fault zone in dolostones: the Foiana Fault Zone (Southern Alps, Italy). Tectonophysics 654, 56–74.
Fondriest, M., Doan, M.L., Aben, F., Fusseis, F., Mitchell, T.M., Voorn, M., Secco, M., Di Toro, G., 2017. Static versus dynamic fracturing in shallow carbonate fault zones. Earth Planet Sci. Lett. 461, 8–19.
Fondriest, M., Balsamo, F., Bistacchi, A., Clemenzi, L., Demurtas, M., Storti, F., Di Toro, G., 2020. Structural complexity and mechanics of a shallow crustal seismogenic source (Vado di Corno Fault Zone, Italy). J. Geophys. Res. Solid Earth 125 (9), e2019JB018926.
Frost, E., Dolan, J., Sammis, C., Hacker, B., Cole, J., Ratschbacher, L., 2009. Progressive strain localization in a major strike-slip fault exhumed from mid seismogenic depths: structural observations from the Salzach-Ennstal-Mariazell-Puchberg fault system, Austria. J. Geophys. Res. Solid Earth 114 (B4).
Galadini, F., Galli, P., 2000. Active tectonics in the central Apennines (Italy)-input data for seismic hazard assessment. Nat. Hazards 22 (3), 225.
Galadini, F., Messina, P., 2004. Early–Middle pleistocene eastward migration of the abruzzi apennine (central Italy) extensional domain. J. Geodyn. 37 (1), 57–81.
Galli, P.A., Giaccio, B., Messina, P., Peronace, E., Zuppi, G.M., 2011. Palaeoseismology of the L'Aquila faults (central Italy, 2009, M w 6.3 earthquake): implications for active fault linkage. Geophys. J. Int. 187 (3), 1119–1134.
Ghisetti, F., Vezzani, L., 1999. Depth and modes of pliocene–pleistocene crustal extension of the Apennines (Italy). Terra. Nova 11 (2-3), 67–72.
Gratier, J.P., Dysthe, D.K., Renard, F., 2013. The role of pressure solution creep in the ductility of the Earth's upper crust. Adv. Geophys. 54, 47–179.
Griffith, W.A., Prakash, V., 2015. Integrating field observations and fracture mechanics models to constrain seismic source parameters for ancient earthquakes. Geology 43 (9), 763–766.
Griffith, W.A., Rosakis, A., Pollard, D.D., Ko, C.W., 2009. Dynamic rupture experiments elucidate tensile crack development during propagating earthquake ruptures. Geology 37 (9), 795–798.
Griffith, W.A., St Julien, R.C., Ghaffari, H.O., Barber, T.J., 2018. A tensile origin for fault rock pulverization. J. Geophys. Res. Solid Earth 123 (8), 7055–7073.
Hausegger, S., Kurz, W., Rabitsch, R., Kiechl, E., Brosch, F.J., 2010. Analysis of the internal structure of a carbonate damage zone: implications for the mechanisms of fault breccia formation and fluid flow. J. Struct. Geol. 32 (9), 1349–1362.
Heilbronner, R., Keulen, N., 2006. Grain size and grain shape analysis of fault rocks. Tectonophysics 427 (1–4), 199–216.
Hesse, M., Asetre, P., Anderson, R., Edwards, C., Lee, C., Malpica, O., Klein, B., 2022. Experimental demonstration of comminution with transcritical carbon diox-ide cycles. Powder 407, 117615. https://doi.org/10.1016/j.powtec.2022.117615.
Huang, Y., Ampuero, J.P., Helmberger, D.V., 2014. Earthquake ruptures modulated by waves in damaged fault zones. J. Geophys. Res. Solid Earth 119 (4), 3133–3154.
Keulen, N., Heilbronner, R., Stünitz, H., Boullier, A.M., Ito, H., 2007. Grain size distributions of fault rocks: a comparison between experimentally and naturally deformed granitoids. J. Struct. Geol. 29 (8), 1282–1300.
Kim, Y.S., Peacock, D.C., Sanderson, D.J., 2004. Fault damage zones. J. Struct. Geol. 26 (3), 503–517.
Kostakioti, A., Xypolias, P., Kokkalas, S., Doutsos, T., 2004. Quantitative analysis of deformation along the fault damage zone of the Klimatia thrust (NW Greece, Ionian Zone). Bull. Geol. Soc. Greece 36 (4), 1643–1651.
Lavecchia, G., Ferrarini, F., Brozzetti, F., De Nardis, R., Boncio, P., Chiaraluce, L., 2012. From surface geology to aftershock analysis: constraints on the geometry of the L'Aquila 2009 seismogenic fault system. Italian J. Geosci. 131 (3), 330–347.
Lavecchia, G., Bello, S., Andrenacci, C., Cirillo, D., Ferrarini, F., Vicentini, N., et al., 2022. QUaternary fault strain INdicators database-QUIN 1.0-first release from the Apennines of central Italy. Sci. Data 9 (1), 204.
Leah, H., Fondriest, M., Lucca, A., Storti, F., Balsamo, F., Di Toro, G., 2018. Coseismic extension recorded within the damage zone of the Vado di Ferruccio Thrust Fault, Central Apennines, Italy. J. Struct. Geol. 114, 121–138.
Lucca, A., Storti, F., Balsamo, F., Clemenzi, L., Fondriest, M., Burgess, R., Di Toro, G., 2019. From submarine to subaerial out-of-sequence thrusting and gravity-driven extensional faulting: gran Sasso Massif, Central Apennines, Italy. Tectonics 38 (12), 4155–4184.
Ma, S., 2009. Distinct asymmetry in rupture-induced inelastic strain across dipping faults: an off-fault yielding model. Geophys. Res. Lett. 36, 20.
Mandelbrot, B., 1977. Fractals: Form, Chance, and Dimension. W.H. Freeman, San Francisco, p. 365.
McGrath, A.G., Davison, I., 1995. Damage zone geometry around fault tips. J. Struct. Geol. 17 (7), 1011–1024.
Micarelli, L., Moretti, I., Daniel, J.M., 2003. Structural properties of rift-related normal faults: the case study of the Gulf of Corinth, Greece. J. Geodyn. 36 (1–2), 275–303.
Micarelli, L., Benedicto, A., Wibberley, C.A.J., 2006. Structural evolution and permeability of normal fault zones in highly porous carbonate rocks. J. Struct. Geol. 28 (7), 1214–1227.
Mitchell, T.M., Ben-Zion, Y., Shimamoto, T., 2011. Pulverized fault rocks and damage asymmetry along the Arima-Takatsuki Tectonic Line, Japan. Earth Planet Sci. Lett. 308 (3–4), 284–297.
Mitchell, T.M., Billi, A., Miller, S.A., Goldsby, D.L., Scholz, C.H., Gran, J.K., Simons, J., 2013. Dynamic pulverization by rapid decompression. Eos Transactions AGU, Fall Meeting Supplement, Abstract MR41B–04.
Moro, M., Bosi, V., Galadini, F., Galli, P., Giaccio, B., Messina, P., Sposato, A., 2002. Analisi paleosismologiche lungo la faglia del M. Marine (alta valle dell'Aterno): risultati preliminari. Il Quaternario. Italian J. Quaternary Sci. 15, 259–270.
Moro, M., Falcucci, E., Gori, S., Saroli, M., Galadini, F., 2016. New paleoseismic data across the Mt. Marine Fault between the 2016 Amatrice and 2009 L'Aquila seismic sequences (central Apennines). Annals of Geophisycs 59 (5), 1–7.
Mort, K., Woodcock, N.H., 2008. Quantifying fault breccia geometry: Dent fault, NW England. Journal of Structural Geology. 30 (6), 701–709.

Muto, J., Nakatani, T., Nishikawa, O., Nagahama, H., 2015. Fractal particle size distribution of pulverized fault rocks as a function of distance from the fault core. Geophys. Res. Lett. 42 (10), 3811–3819.
Ni, T., Pesavento, F., Zaccariotto, M., Galvanetto, U., Schrefler, B.A., 2021. Numerical simulation of forerunning fracture in saturated porous solids with hybrid fem/peridynamic model. Comput. Geotech. 133, 104024.
Niemeijer, A.R., Spiers, C.J., 2006. Velocity dependence of strength and healing behaviour in simulated phyllosilicate-bearing fault gouge. Tectonophysics 427 (1–4), 231–253.
Okubo, K., Bhat, H.S., Rougier, E., Marty, S., Schubnel, A., Lei, Z., et al., 2019. Dynamics, radiation, and overall energy budget of earthquake rupture with coseismic off-fault damage. J. Geophys. Res. Solid Earth 124. https://doi.org/10.1029/2019JB017304.
Ostermeijer, G.A., Aben, F.M., Mitchell, T.M., Rockwell, T.K., Rempe, M., Farrington, K., 2022. Evolution of co-seismic off-fault damage towards pulverisation. Earth Planet Sci. Lett. 579, 117353.
Passelègue, F.X., Aubry, J., Nicolas, A., Fondriest, M., Deldicque, D., Schubnel, A., Di Toro, G., 2019. From fault creep to slow and fast earthquakes in carbonates. Geology 47 (8), 744–748.
Payne, R.M., Duan, B., 2017. Insights into pulverized rock formation from dynamic rupture models of earthquakes. Geophys. J. Int. 208 (2), 715–723.
Pizzi, A., Di Domenica, A., Gallovič, F., Luzi, L., Puglia, R., 2017. Fault segmentation as constraint to the occurrence of the main shocks of the 2016 Central Italy seismic sequence. Tectonics 36 (11), 2370–2387.
Poliakov, A.N.B., Dmowska, R., Rice, J.R., 2002. Dynamic shear rupture interactions with fault bends and off-axis secondary faulting. J. Geophys. Res. 107 (B11), 2295. https://doi.org/10.1029/2001JB000572.
Pucci, S., Villani, F., Civico, R., Di Naccio, D., Porreca, M., Benedetti, L., et al., 2019. Complexity of the 2009 L'Aquila earthquake causative fault system (Abruzzi Apennines, Italy) and effects on the Middle Aterno Quaternary basin arrangement. Quat. Sci. Rev. 213, 30–66.
Rawling, G.C., Goodwin, L.B., 2003. Cataclasis and particulate flow in faulted, poorly lithified sediments. J. Struct. Geol. 25 (3), 317–331.
Rempe, M., Mitchell, T., Renner, J., Nippress, S., Ben-Zion, Y., Rockwell, T., 2013. Damage and seismic velocity structure of pulverized rocks near the San Andreas Fault. J. Geophys. Res. Solid Earth 118 (6), 2813–2831.
Renard, F., Gratier, J.P., Jamveit, B., 2000. Kinetics of crack-sealing, intergranular pressure solution, and compaction around active faults. J. Struct. Geol. 22 (10), 1395–1407.
Renard, F., Cordonnier, B., Doan, M.L., Fondriest, M., Lukic, B., Prastyani, E., 2023. Dynamic damage in dry and wet rocks monitored by ultra-fast synchrotron imaging. In: Conference Paper, European Geophysical Union.
Rockwell, T., Sisk, M., Girty, G., Dor, O., Wechsler, N., Ben-Zion, Y., 2009. Chemical and physical characteristics of pulverized Tejon Lookout granite adjacent to the San Andreas and Garlock faults: implications for earthquake physics. Pure Appl. Geophys. 166, 1725–1746.
Rowe, C.D., Griffith, W.A., 2015. Do faults preserve a record of seismic slip: a second opinion. J. Struct. Geol. 78, 1–26.
Sammis, C., King, G., Biegel, R., 1987. The kinematics of gouge deformation. Pure Appl. Geophys. 125, 777–812.
Savage, H.M., Brodsky, E.E., 2011. Collateral damage: evolution with displacement of fracture distribution and secondary fault strands in fault damage zones. J. Geophys. Res. Solid Earth 116 (B3).
Schneider, C.A., Rasband, W.S., Eliceiri, K.W., 2012. NIH Image to ImageJ: 25 years of image analysis. Nat. Methods 9 (7), 671–675. https://doi.org/10.1038/nmeth.2089.
Schröckenfuchs, T., Bauer, H., Grasemann, B., Decker, K., 2015. Rock pulverization and localization of a strike-slip fault zone in dolomite rocks (Salzach–Ennstal–Mariazell–Puchberg fault, Austria). J. Struct. Geol. 78, 67–85.
Servizio Geologico d'Italia, 2022. Geological map of Italy at the scale 1:50.000, F. 348. Antrodoco. ISPRA, Roma. https://doi.org/10.15161/oar.it/75554. Available at.
Servizio Geologico d'Italia, 2010. Geological Map of Italy at the Scale 1:50.000, F. 349. Gran Sasso d'Italia. ISPRA, Roma. Available at. https://www.isprambiente.gov.it/Media/carg/349_GRANSASSO/Foglio.html.
Sibson, R.H., 1974. Frictional constraints on thrust, wrench and normal faults. Nature 249, 542–544.
Sibson, R.H., 1977. Fault rocks and fault mechanisms. J. Geol. Soc. 133 (3), 191–213.
Smith, Z.D., Griffith, W.A., 2022. Evolution of pulverized fault zone rocks by dynamic tensile loading during successive earthquakes. Geophys. Res. Lett. 49 (19), e2022GL099971.
Smith, S.A.F., Billi, A., Toro, G.D., Spiess, R., 2011. Principal slip zones in limestone: microstructural characterization and implications for the seismic cycle (Tre Monti Fault, Central Apennines, Italy). Pure Appl. Geophys. 168, 2365–2393.
Smith, S.A.F., Griffiths, J.R., Fondriest, M., Di Toro, G., 2017. "Coseismic foliations" in gouge and cataclasite: experimental observations and consequences for interpreting the fault rock record. In: Thomas, M.Y., Mitchell, T.M., Bhat, H.S. (Eds.), Fault Zone Dynamic Processes: Evolution of Fault Properties during Seismic Rupture, vol. 227. American Geophysical Union, Geophysical Monograph, pp. 81–102.
Socquet, A., Hollingsworth, J., Pathier, E., Bouchon, M., 2019. Evidence of supershear during the 2018 magnitude 7.5 Palu earthquake from space geodesy. Nat. Geosci. 12 (3), 192–199.
Solum, J.G., Huisman, B.A.H., 2017. Toward the creation of models to predict static and dynamic fault-seal potential in carbonates. Petrol. Geosci. 23 (1), 70–91.
Storti, F., Balsamo, F., 2010. Particle size distributions by laser diffraction: sensitivity of granular matter strength to analytical operating procedures. Solid Earth 1 (1), 25–48.
Storti, F., Billi, A., Salvini, F., 2003. Particle size distributions in natural carbonate fault rocks: insights for non-self-similar cataclasis. Earth Planet Sci. Lett. 206 (1–2), 173–186.
Storti, F., Balsamo, F., Salvini, F., 2007. Particle shape evolution in natural carbonate granular wear material. Terra. Nova 19 (5), 344–352.
Tondi, E., Cello, G., 2003. Spatiotemporal evolution of the Central Apennines fault system (Italy). J. Geodyn. 36 (1–2), 113–128.
Turcotte, D.L., 1986. Fractals and fragmentation. J. Geophys. Res. Solid Earth 91 (B2), 1921–1926.
Valoroso, L., Chiaraluce, L., Collettini, C., 2014. Earthquakes and fault zone structure. Geology 42 (4), 343–346.
Valoroso, L., Chiaraluce, L., Piccinini, D., Di Stefano, R., Schaff, D., Waldhauser, F., 2013. Radiography of a normal fault system by 64,000 high-precision earthquake locations: The 2009 L'Aquila (central Italy) case study. J. Geophys. Res: Solid Earth 118 (3), 1156–1176.
Verberne, B.A., Plümper, O., Matthijs de Winter, D.A., Spiers, C.J., 2014. Superplastic nanofibrous slip zones control seismogenic fault friction. Science 346 (6215), 1342–1344.
Vezzani, L., Ghisetti, F., 1998. Carta Geologica dell'Abruzzo, Scale 1:100,000. S. EL.CA., Firenze.
Wentworth, C.K., 1922. A scale of grade and class terms for clastic sediments. J. Geol. 30 (5), 377–392.
Whearty, J.J., Rockwell, T.K., Girty, G.H., 2017. Incipient pulverization at shallow burial depths along the san jacinto fault, southern California. In: Thomas, M.Y., Mitchell, T. M., Bhat, H.S. (Eds.), Fault Zone Dynamic Processes: Evolution of Fault Properties during Seismic Rupture, vol. 227. American Geophysical Union, Geophysical Monograph, pp. 1–20.
Williams, R.T., Rowe, C.D., Okamoto, K., Savage, H.M., Eves, E., 2021. How fault rocks form and evolve in the shallow San Andreas fault. G-cubed 22 (11), e2021GC010092.
Xu, S., Ben-Zion, Y., 2017. Theoretical constraints on dynamic pulverization of fault zone rocks. Geophys. J. Int. 209 (1), 282–296.
Yao, W., Xu, Y., Xia, K., 2020. Damage evolution during rock pulverization induced by dynamic compressive loading. J. Geophys. Res: Solid Earth 125 e2020JB019388.